

Combined Analysis: XRD – XRF – Raman within the EU-SOLSA Project

D. Chateigner, L. Lutterotti, and the SOLSA Consortium



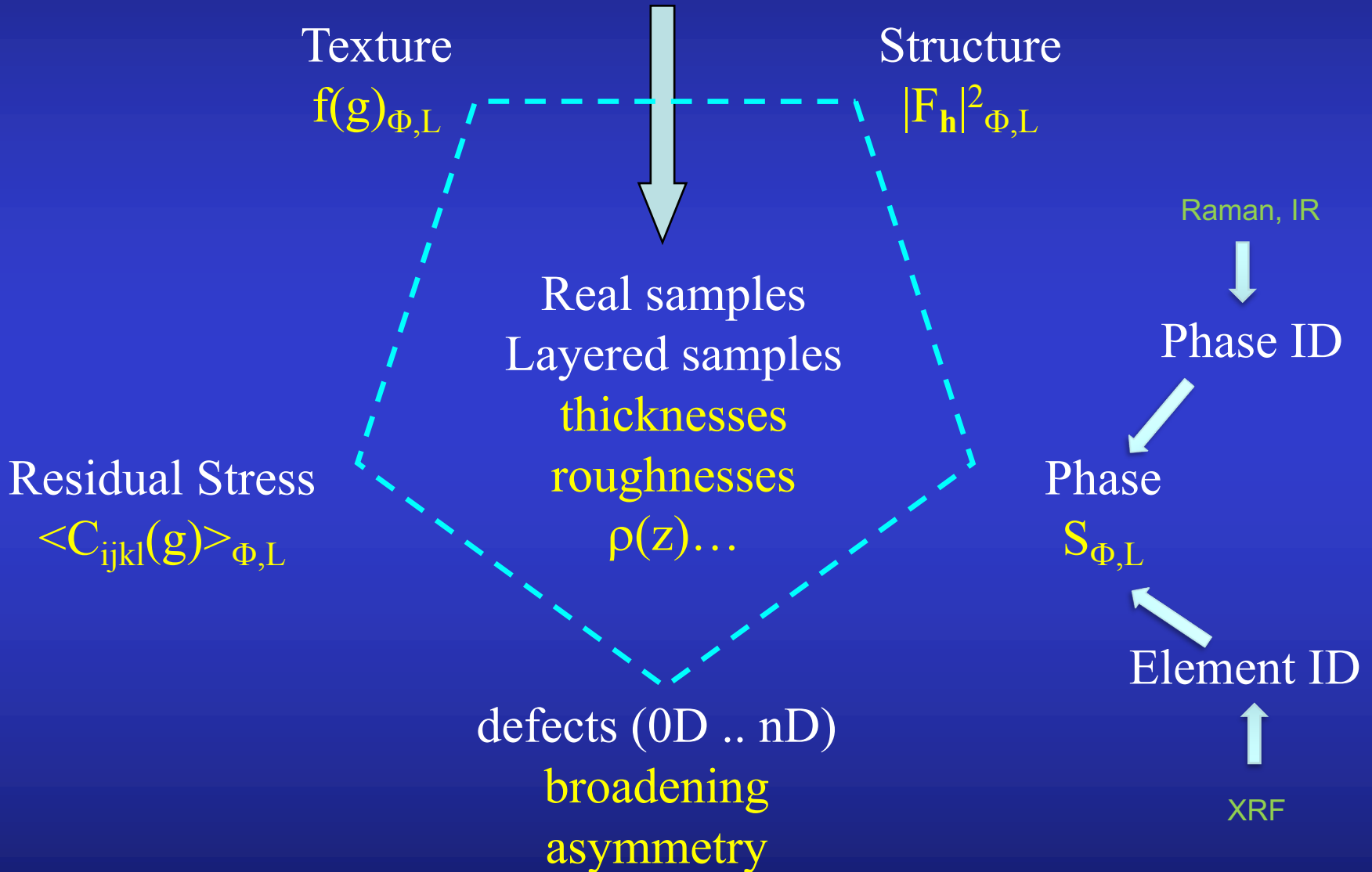
Normandie Université, Università di Trento

Normandie Université



Crystallography, Roma, Italy, 25-26th Apr. 2019

Scattering “sees”



Rietveld: Acta Cryst. (1967), J. Appl. Cryst (1969)

computers, neutrons (Gaussian peaks): powders !

Lutterotti, Matthies, Wenk: Rietveld Texture Analysis, J. Appl. Phys. (1997)

classical Rietveld + QTA (WIMV)

Morales, Chateigner, Lutterotti, Ricote: Mat. Sci. For. (2002)

Rietveld of layers (QTA, QMA) + E-WIMV

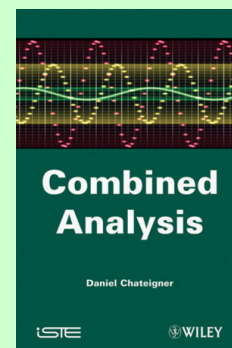
ESQUI EU FP6 project (ended Jan. 2003)

Lutterotti, Chateigner, Ferrari, Ricote: Thin Sol. Films (2004)

E-WIMV + RSA + XRR + Geom. Mean: Extended Rietveld

Chateigner, Combined Analysis, Wiley-ISTE (2010)

International Tables Vol H (2019)



Boullay, Lutterotti, Chateigner, Sicard: Acta Cryst A (2014)

Electron Diffraction Pattern – 2-waves Blackman correction

Rietveld: extended to lots of spectra

$$y_c(\mathbf{y}_S, \theta, \eta) = y_b(\mathbf{y}_S, \theta, \eta) + I_0 \sum_{i=1}^{N_L} \sum_{\Phi=1}^{N_\Phi} \frac{v_{i\Phi}}{V_{c\Phi}} \sum_h L_p(\theta) j_{\Phi h} |F_{\Phi h}|^2 \Omega_{\Phi h}(\mathbf{y}_S, \theta, \eta) P_{\Phi h}(\mathbf{y}_S, \theta, \eta) A_{i\Phi}(\mathbf{y}_S, \theta, \eta)$$

Texture:

$$P_h(\mathbf{y}_S) = \int_{\tilde{\varphi}} f(\mathbf{g}, \tilde{\varphi}) d\tilde{\varphi}$$

E-WIMV, components,
Harmonics, Exp. Harmonics ...

Strain-Stress:

$$\langle S \rangle_{\text{geo}}^{-1} = \left[\prod_{m=1}^N S_m^{v_m} \right]^{-1} = \prod_{m=1}^N S_m^{-v_m} = \prod_{m=1}^N (S_m^{-1})^{v_m} = \langle S^{-1} \rangle_{\text{geo}} = \langle C \rangle_{\text{geo}}$$

Geometric mean, Voigt, Reuss, Hill ...

Layering:

$$A_{i\Phi} = \frac{v_{i\Phi} \sin \theta_i \sin \theta_o}{\mu_i (\sin \theta_i + \sin \theta_o)} \left\{ 1 - e^{-\bar{\mu}_i \tau_i W} \right\} \prod_{k < i} e^{-\bar{\mu}_k \tau_k W}$$

$$W = \frac{1}{\sin \theta_i} + \frac{1}{\sin \theta_o}$$

Stacks,
coatings,
multilayers ...

Line Broadening:

Popa, Delft: Crystallite sizes, shapes, microstrains, distributions
0D-3D defects

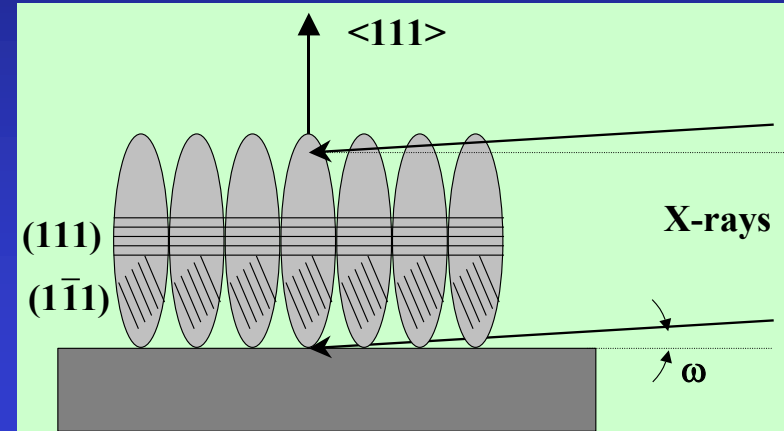
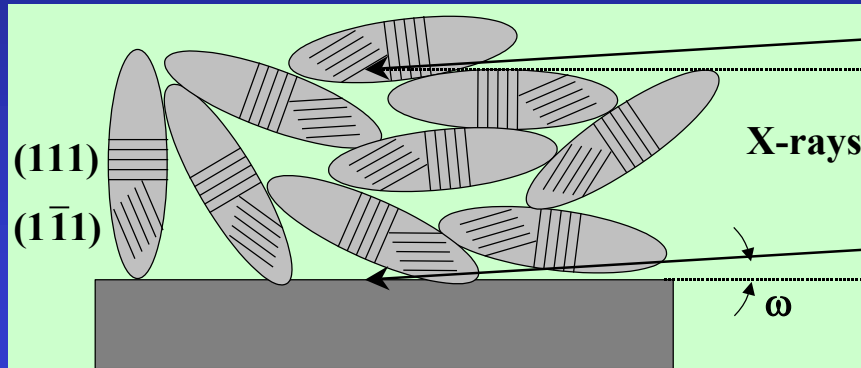
X-Ray Reflectivity (specular): Matrix, Parrat, DWBA, EDP ...

X-Ray Fluorescence/GiXRF: De Boer

Electron Diffraction Patterns: 2-waves Blackman

Line Broadening:

Crystallite sizes, shapes, μ strains, distributions



- Texture helps the "real" mean shape determination

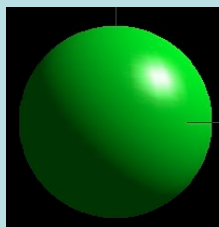
$$\langle R_{\vec{h}} \rangle = \sum_{l=0}^L \sum_{m=0}^l R_l^m K_l^m(\chi, \varphi)$$

Symmetrised spherical harmonics

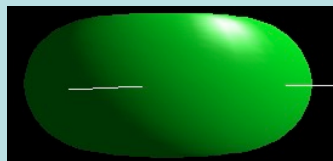
$$K_l^m(\chi, \varphi) = P_l^m(\cos \chi) \cos(m\varphi) + P_l^m(\cos \chi) \sin(m\varphi)$$

$$\begin{aligned} \langle R_{\vec{h}} \rangle &= R_0 + R_1 P_2^0(x) + R_2 P_2^1(x) \cos \varphi + R_3 P_2^1(x) \sin \varphi + R_4 P_2^2(x) \cos 2\varphi + R_5 P_2^2(x) \sin 2\varphi + \\ \langle \epsilon_{\vec{h}}^2 \rangle E_{\vec{h}}^4 &= E_1 h^4 + E_2 k^4 + E_3 \ell^4 + 2E_4 h^2 k^2 + 2E_5 \ell^2 k^2 + 2E_6 h^2 \ell^2 + 4E_7 h^3 k + 4E_8 h^3 \ell + 4E_9 k^3 h + \\ &\quad 4E_{10} k^3 \ell + 4E_{11} \ell^3 h + 4E_{12} \ell^3 k + 4E_{13} h^2 k \ell + 4E_{14} k^2 h \ell + 4E_{15} \ell^2 k h \end{aligned}$$

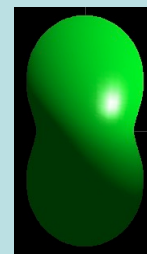
$\bar{1}$



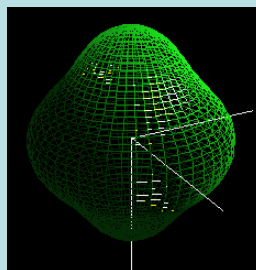
R_0



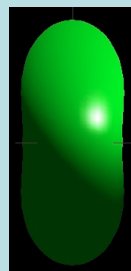
$R_0, R_1 < 0$



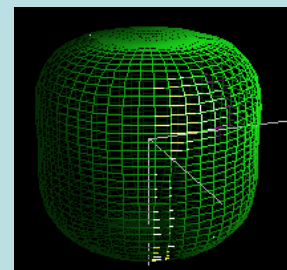
$R_0, R_1 > 0$



$R_0, R_6 > 0$

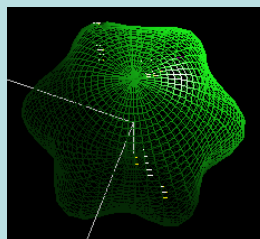


$R_0,$
 R_2 and $R_6 > 0$

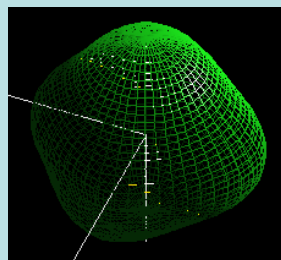


$R_0, R_6 < 0$

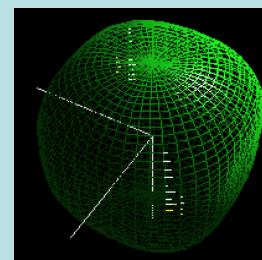
$6/m$



$R_0, R_4 > 0$



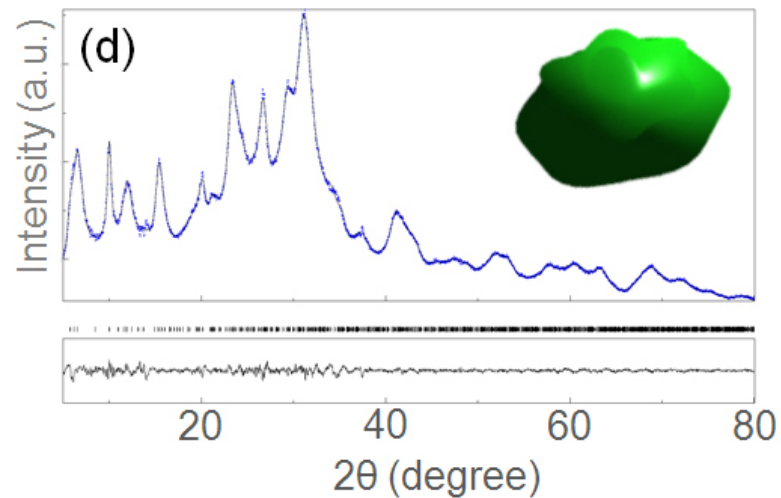
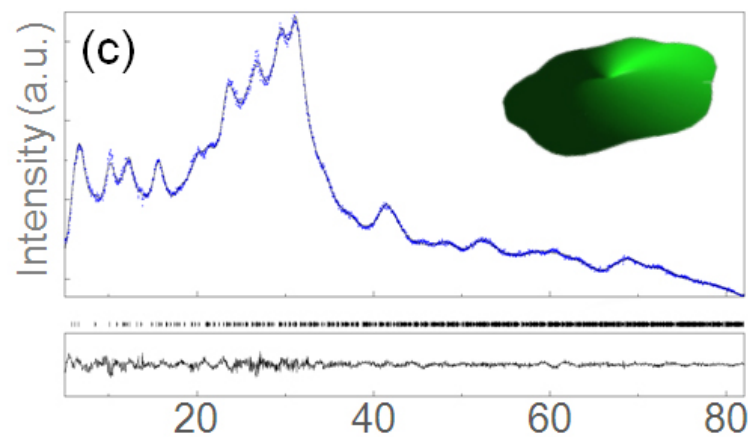
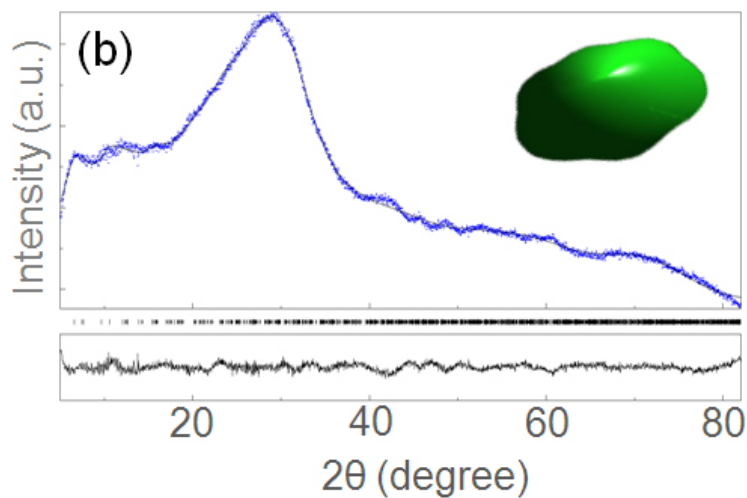
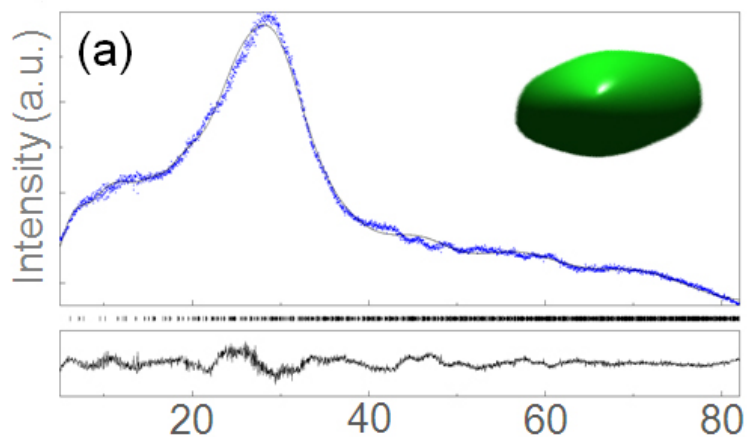
$R_0, R_1 > 0$



$R_0, R_1 < 0$

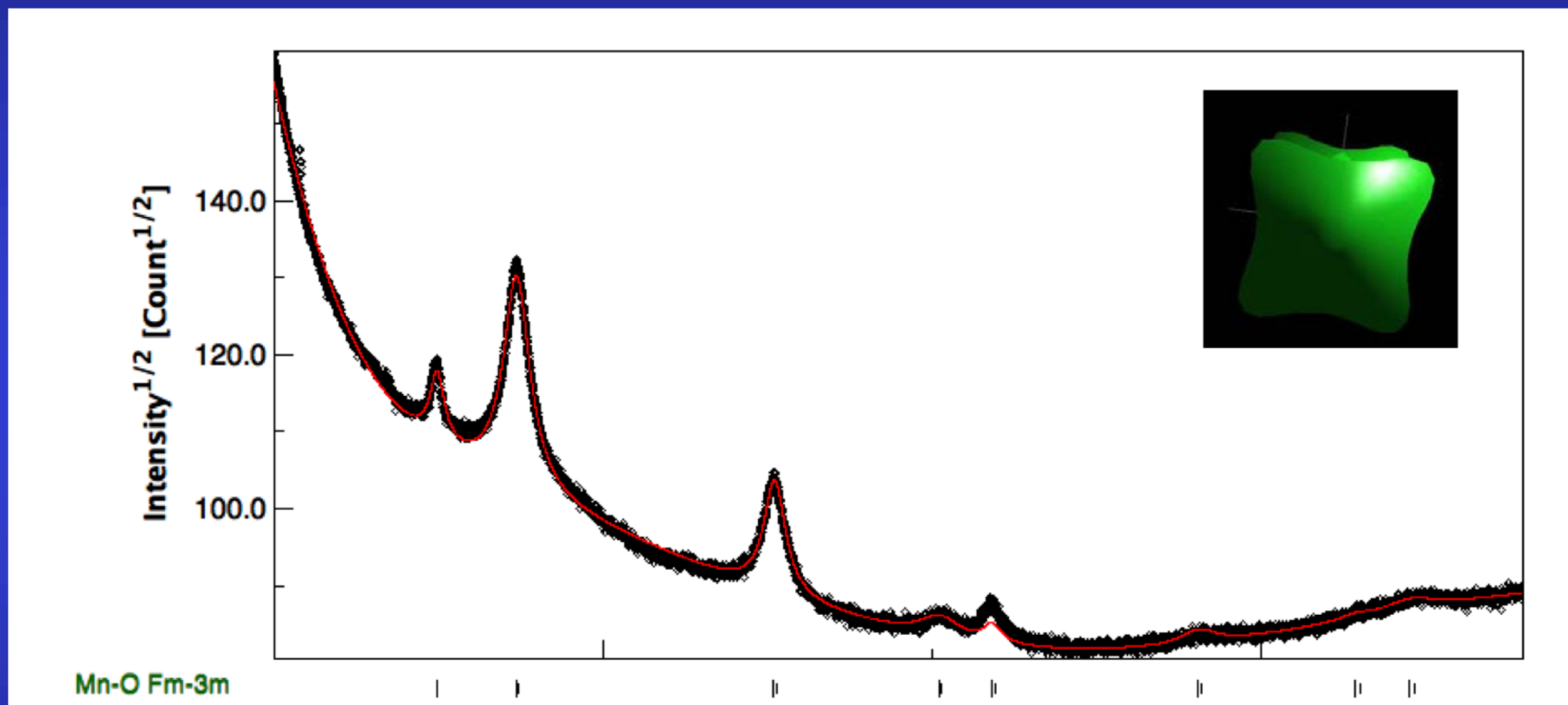
$m\bar{3}m$

EMT nanocrystalline zeolite



Ng, Chateigner, Valtchev, Mintova: *Science* **335** (2012) 70

New active Li–Mn–O compound for high energy density Li-ion batteries

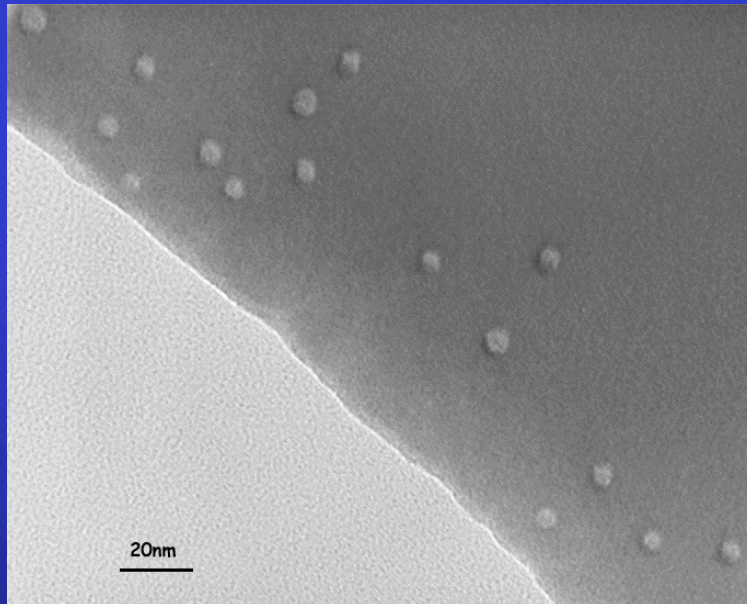


Rock-salt-type nanostructured material: shows a discharge capacity of 355 mAh/g

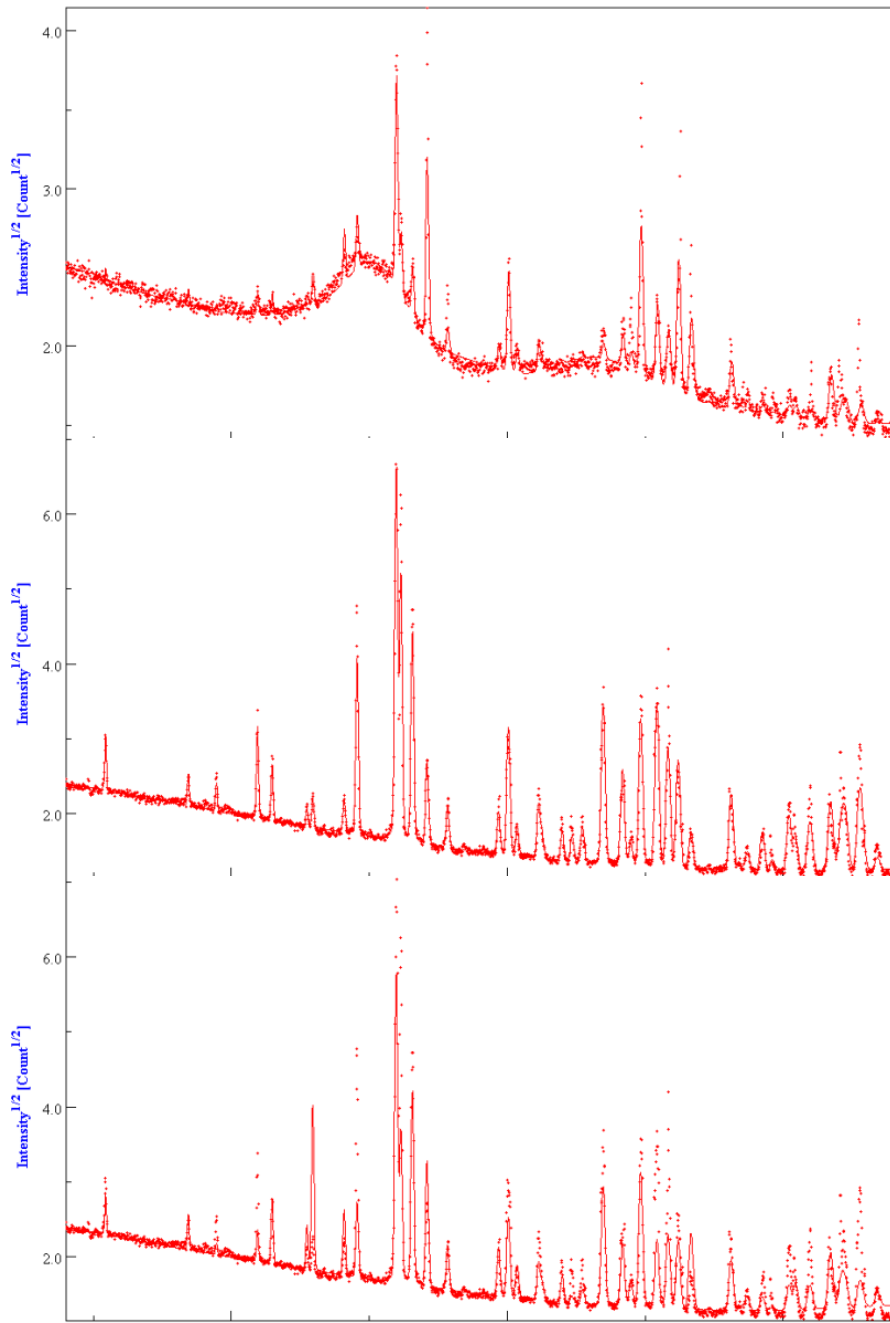
Freire, Kosovab, Jordy, Chateigner, Lebedev, Maignan, Pralong: *Nature Mat.* **15** (2016) 173

Irradiated FluorApatite (FAp) ceramics

Self-recrystallisation under irradiation, depending on $\text{SiO}_4 / \text{PO}_4$ ratio (FAp / Nd-Britholite) and on irradiating species



TEM of FAp
irradiated with 70
MeV, 10^{12} Kr cm^{-2}
ions



Ca5-(P-O4)3-F

texture corrected,
 10^{13} Kr cm⁻²

Virgin, with texture
correction

Virgin, no texture
correction

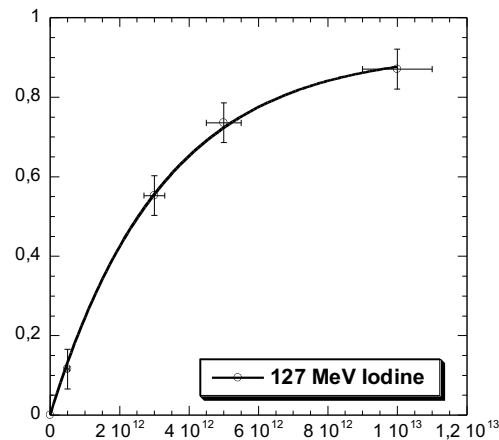
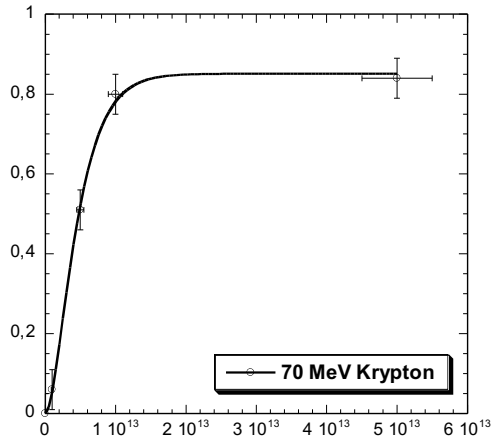
Fluence (ions.cm ⁻²)	Vc/V (%)	A (Å)	c (Å)	<t> (nm)	Δa/a ₀ (%)	Δc/c ₀ (%)	R _w (%)	R _B (%)
0	100	9.3365(3)	6,8560(5)	294(22)	-	-	14.6	9.1
Kr								
10 ¹¹	100	-	-	-	-	-		
10 ¹²	100	-	-	-	-	-		
5.10 ¹²	49(1)	9.3775(9)	6.8912(8)	294(20)	0.44	0.53	24	15
10 ¹³	20(1)	9.4236(5)	6.9105(5)	291(20)	0.94	0.82	9.9	6
5.10 ¹³	14(1)	9.3160(4)	6.8402(5)	294(22)	-0.21	-0.22	10.5	5.9
I								
10 ¹¹	-	-	-	-	-	-		
5.10 ¹¹	86(2)	9.3603(3)	6.8790(5)	90(10)	0.26	0.35	23.9	15.1
10 ¹²	-	-	-	-	-	-		
3.10 ¹²	47(2)	9.3645(3)	6.8840(5)	91(6)	0.30	0.42	13.3	9
5.10 ¹²	29.2(5)	9.3765(5)	6.8881(6)	77(11)	0.44	0.48	10.4	7.3
10 ¹³	13.2(2)	9.3719(4)	6.8857(6)	82(9)	0.38	0.45	6.7	4.9

Single impact model associated to crystal size reduction

Cell parameters and volume increase, then relax

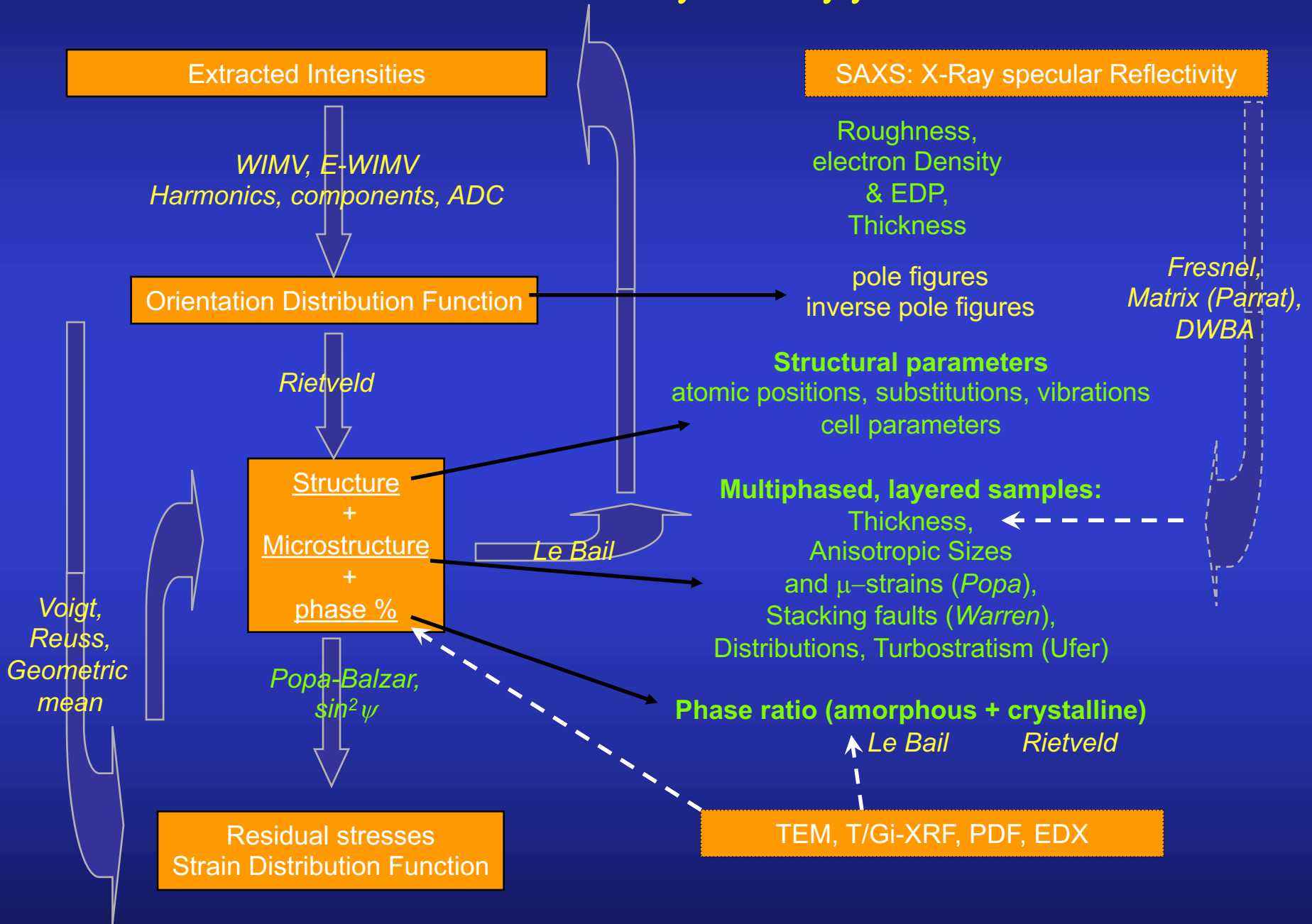
Amorphisation / recrystallisation competition: single or double impact

Amorphous/crystalline volume fraction (damaged fraction $F_d = V_a / V$) as determined by x-ray diffraction



Fitting parameters	Krypton		Iodine
	Single impact	Double impact	Single impact
	$F_d = B(1 - \exp(-A\phi t))$	$F_d = B(1 - (1 + A\phi t) \exp(-A\phi t))$	$F_d = B(1 - \exp(-A\phi t))$
$A = \pi R^2$ (cm ²)	$1.85 \pm 0.15 \cdot 10^{-13}$	$4.1 \pm 0.15 \cdot 10^{-13}$	$3.3 \pm 0.15 \cdot 10^{-13}$
Radius R (nm)	2.4 ± 0.2	3.6	3.2
B (Max.damage rate)	0.87	0.85 ± 0.2	0.92 ± 0.2
χ^2	0.013	0.0006	0.0004

Combined Analysis approach



Minimum experimental requirements

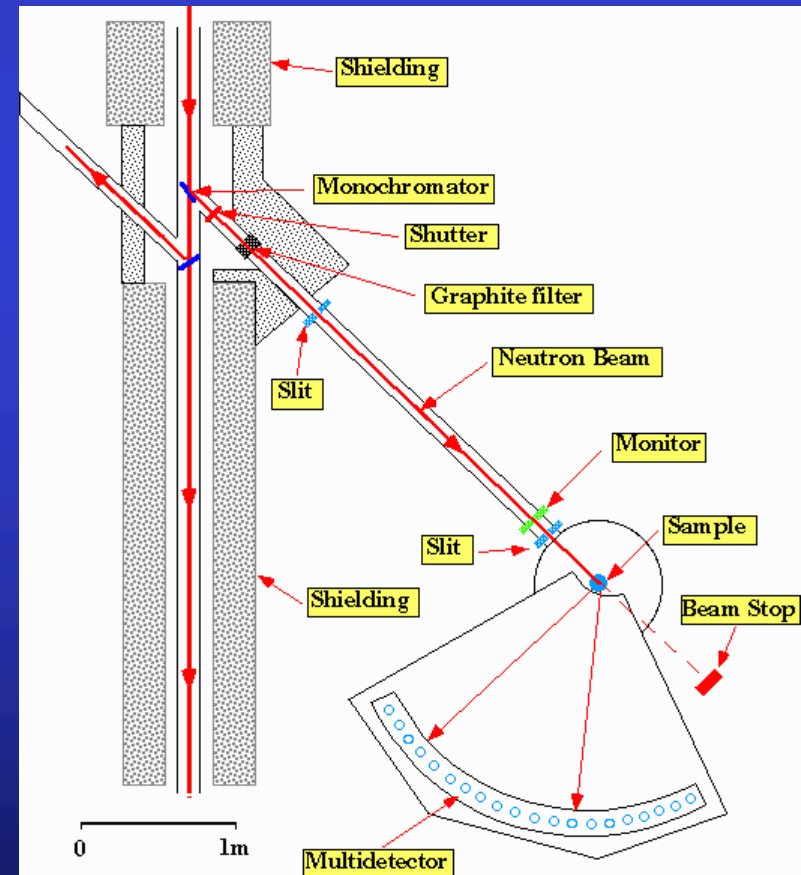
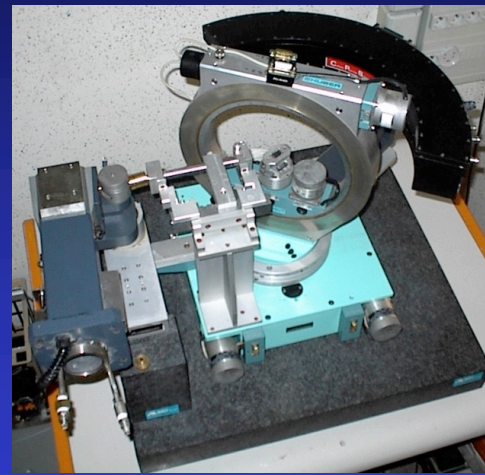
1D or 2D Detector + 4-circle diffractometer
(X-rays and neutrons)
CRISMAT, ILL (B. Ouladdiaf, T. Hansen)

+

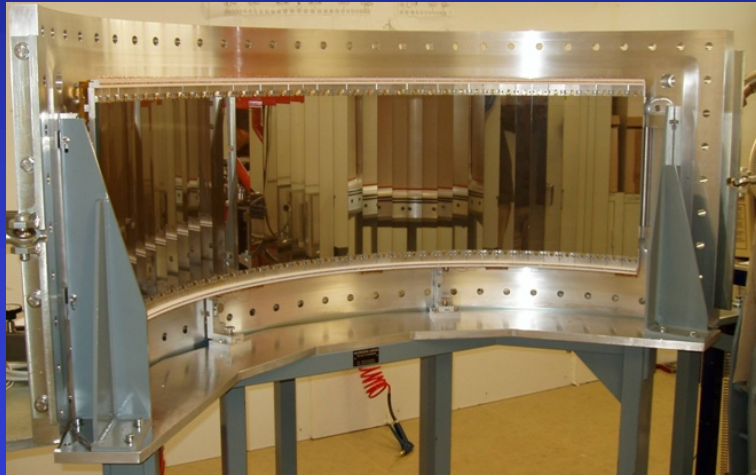
~1000 experiments (2 θ diagrams)
in as many sample orientations

+

Instrument calibration
(peaks widths and shapes,
misalignments, defocusing ...)



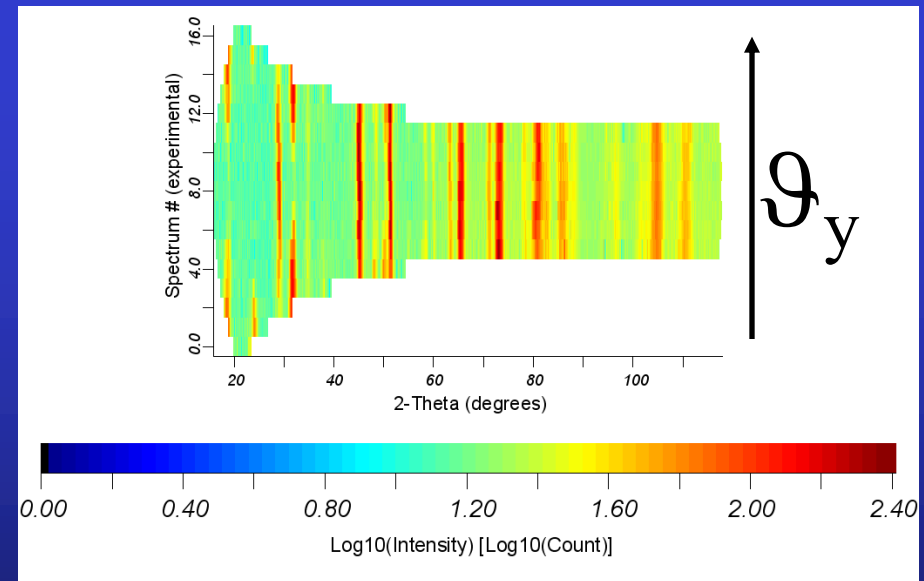
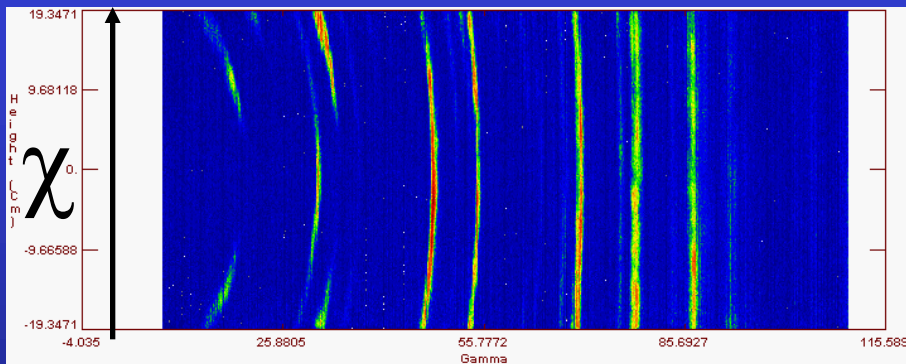
2D Curved Area Position Sensitive Detector



D19 - ILL

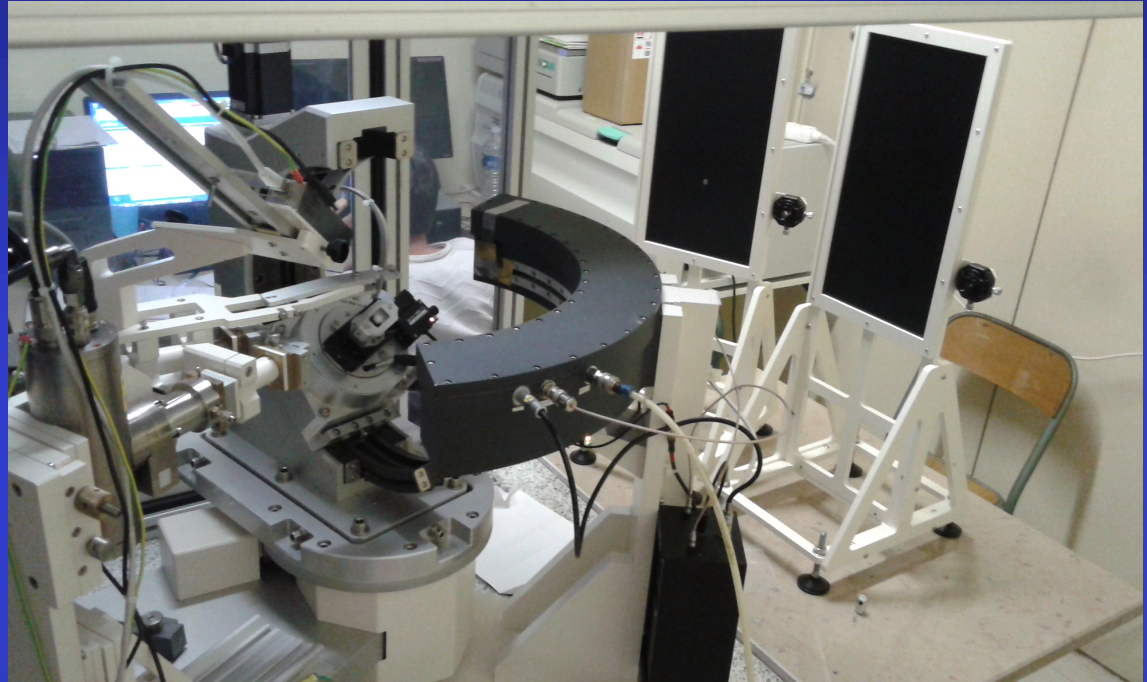
+

~100 experiments (2D Debye-Scherrer diagrams)
in as many sample orientations



Minimum experimental requirements

1D or 2D Detector +
4-circle diffractometer
(CRISMAT – ANR EcoCorail)



~1000 experiments (2θ diagrams)
in as many sample orientations

+

Instrument calibration
(peaks widths and shapes,
misalignments, defocusing ...)

Independent measurements

Different wavelengths and rays

Reflectivity: thickness, roughness, electron density profiles

X-ray Fluorescence: composition

Spectroscopies: local structures (PDF, FTIR, Mossbauer ...), eventually anisotropic (P-EXAFS, ESR, Raman ...), Element profiles (SIMS, RBS ...) ...

Physical models: magnetisation, conductivity ...

Environments: applied fields

Combined Analysis cost function

$$WSS = \sum_{t=1}^{N_p} u_t \sum_{i=0}^{N_t} w_{it} (y_{itc} - y_{ito})^2$$

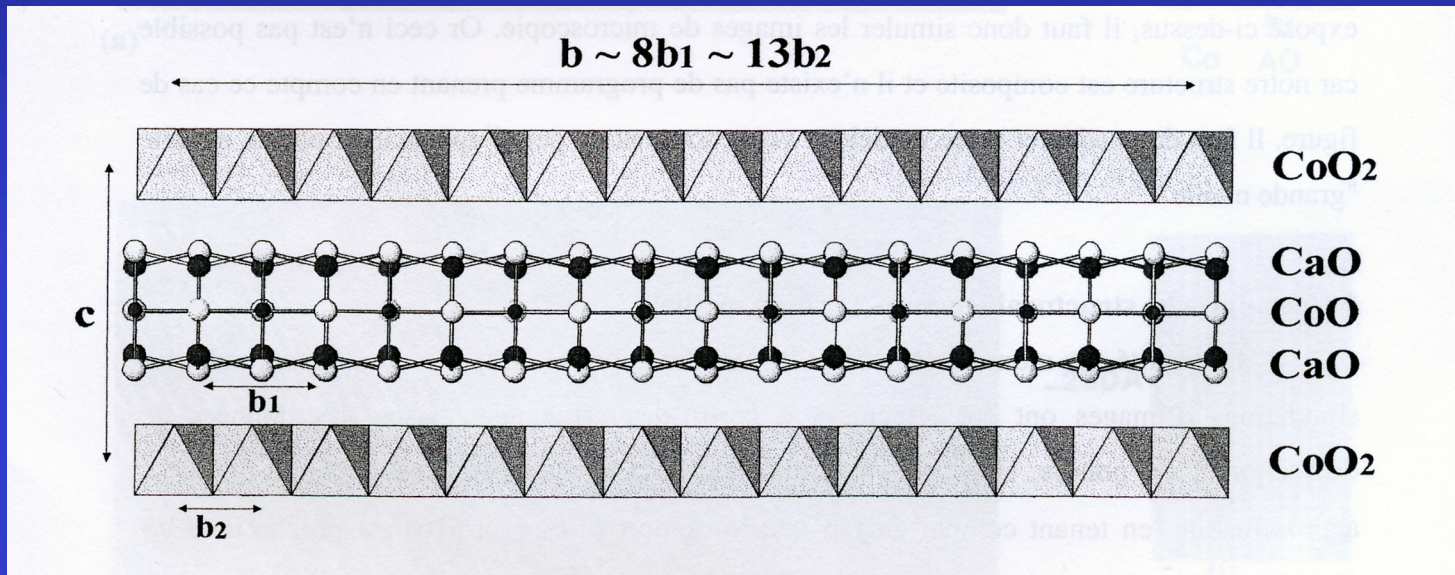
For each pattern t : w_{it} : weight, usually $1/y_i = \sigma^2$.

u_t : weight of each pattern set t

should be used to adjust the importance we want to give to a particular technique or pattern set with respect to the others

Ca₃Co₄O₉ thermoelectrics

Ca₃Co₄O₉: Misfit lamellar and modulated Structure, with high thermopower



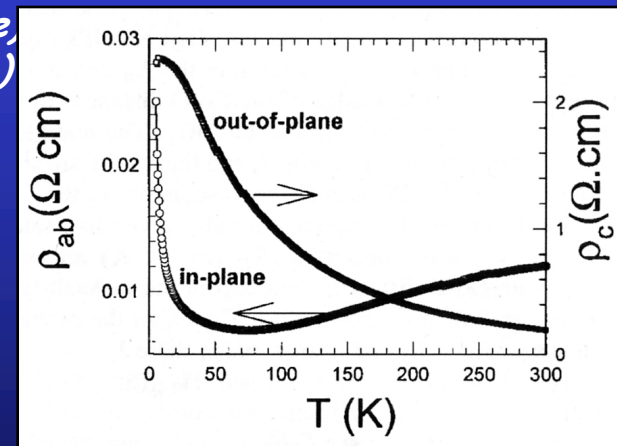
Two monoclinic sub-systems:

S1 with $a \sim 4.8\text{\AA}$, $b_1 \sim 4.5\text{\AA}$, $c \sim 10.8\text{\AA}$ et $\beta \sim 98^\circ$ (NaCl-type),
 S2 with $a \sim 4.8\text{\AA}$, $b_2 \sim 2.8\text{\AA}$, $c \sim 10.8\text{\AA}$ et $\beta \sim 98^\circ$ (CdI₂-type)

$$\Gamma = \sigma_{ab} / \sigma_c \sim 10$$



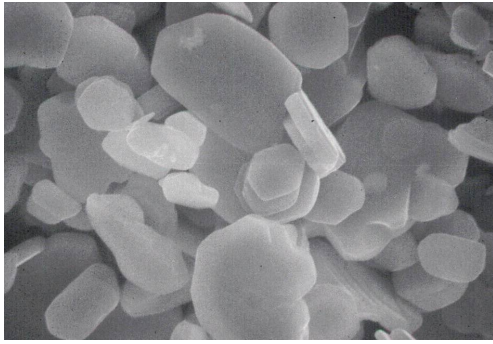
Texture



Magnetic alignment + Templated Growth

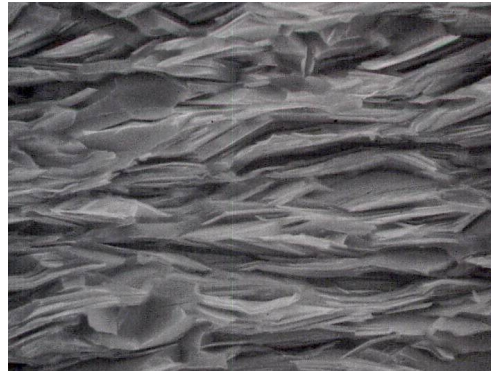
D. Kenfaui, E. Guilmeau, M. Prevel

powder

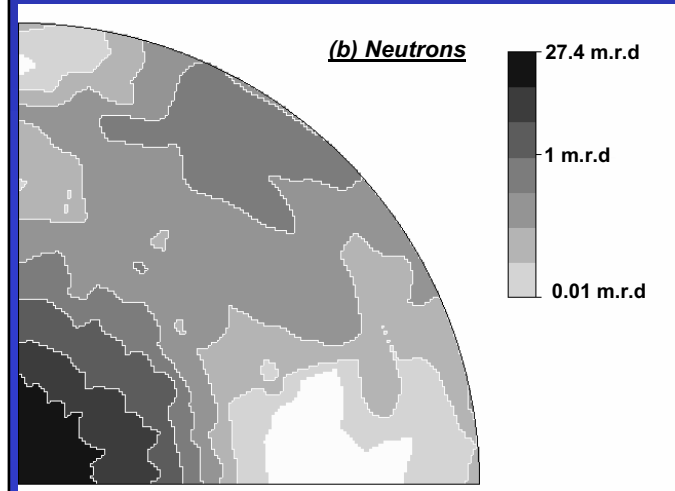


10 μm

Textured bulk



10 μm

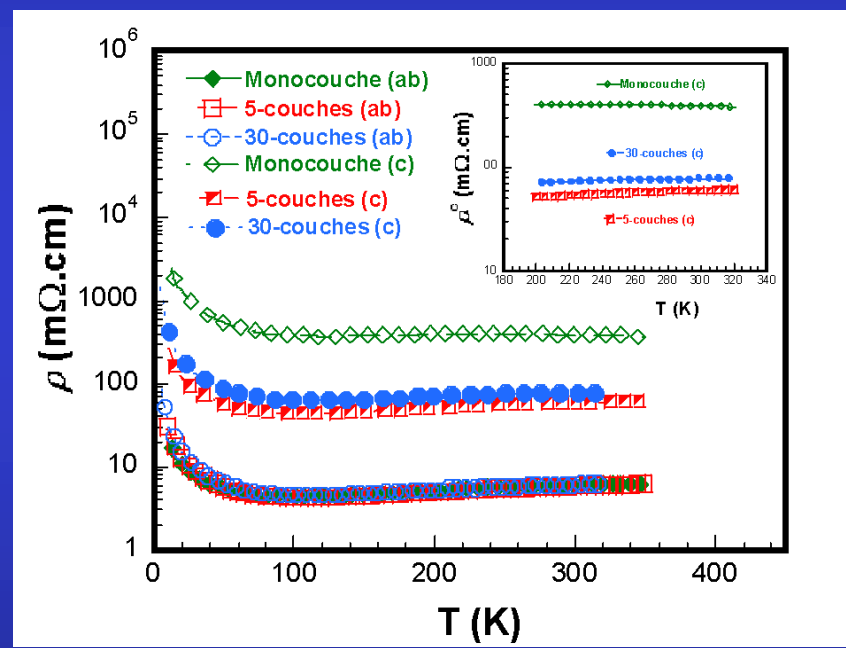
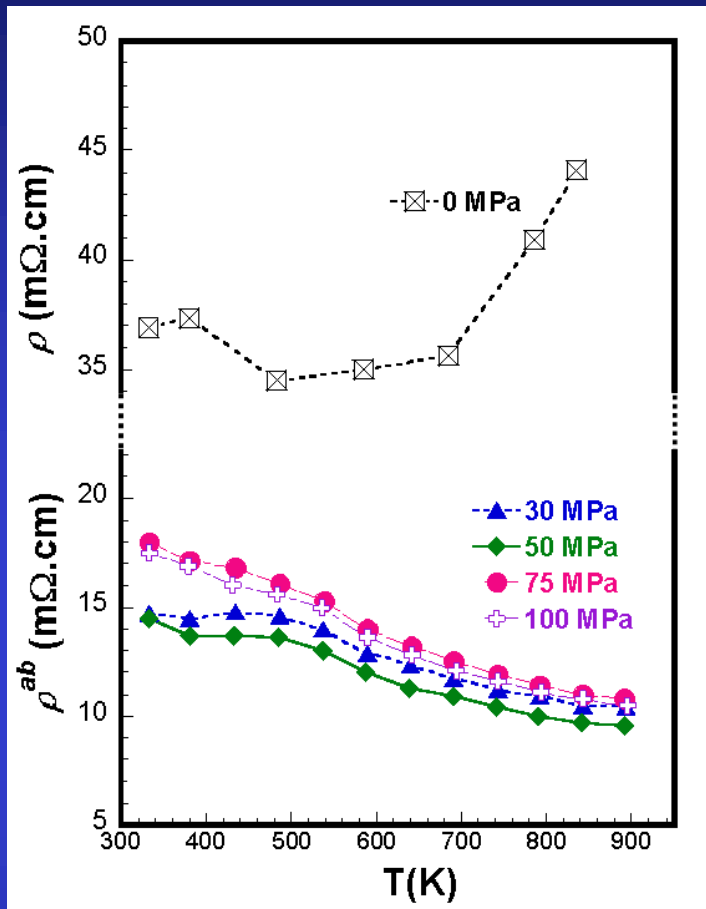
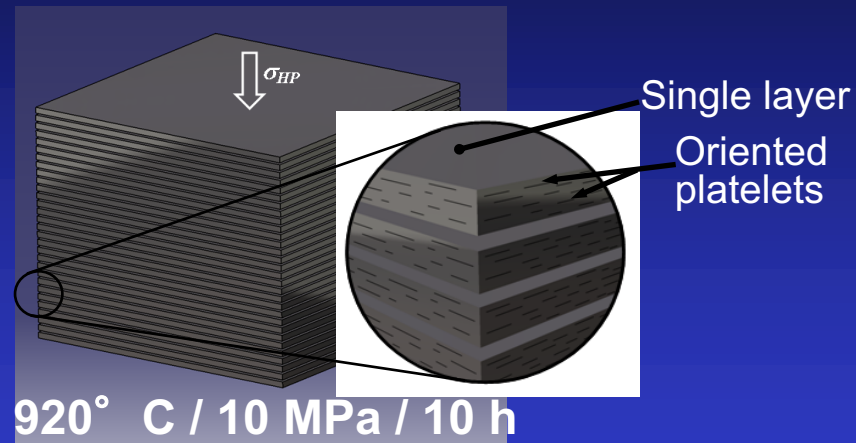


- Neutrons @D1B

- 3D Supercell: $a=4.8309\text{\AA}$, $b\sim 8b_1\sim 13b_2\sim 36.4902\text{\AA}$, $c=10.8353\text{\AA}$, $\beta=98.13^\circ$

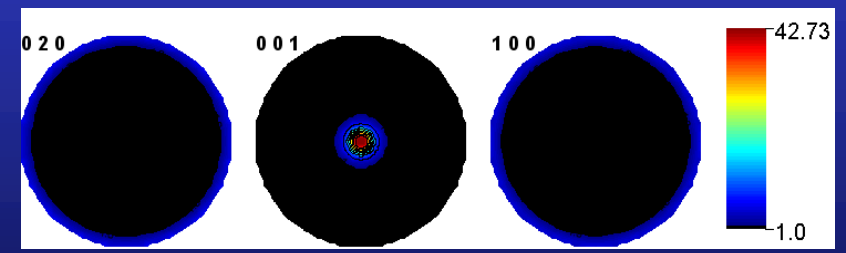
174 atoms/cell

-Sample : 0.6 cm^3

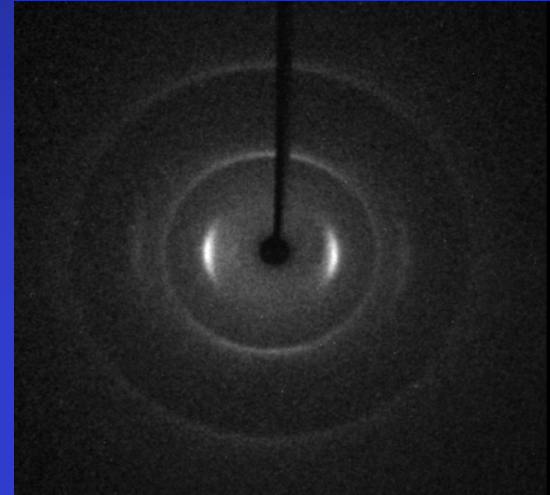
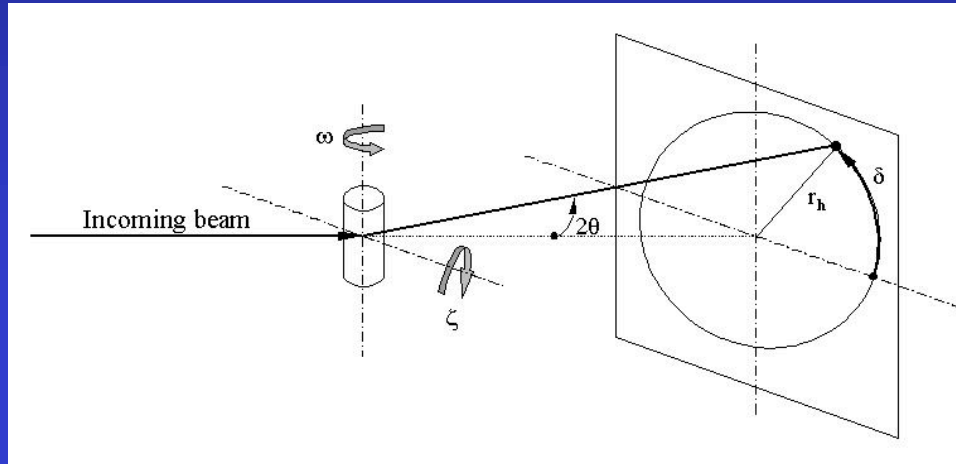


□ Texture

- neutrons @D1B
- volume texture
- max. {001} : 42.73 mrd

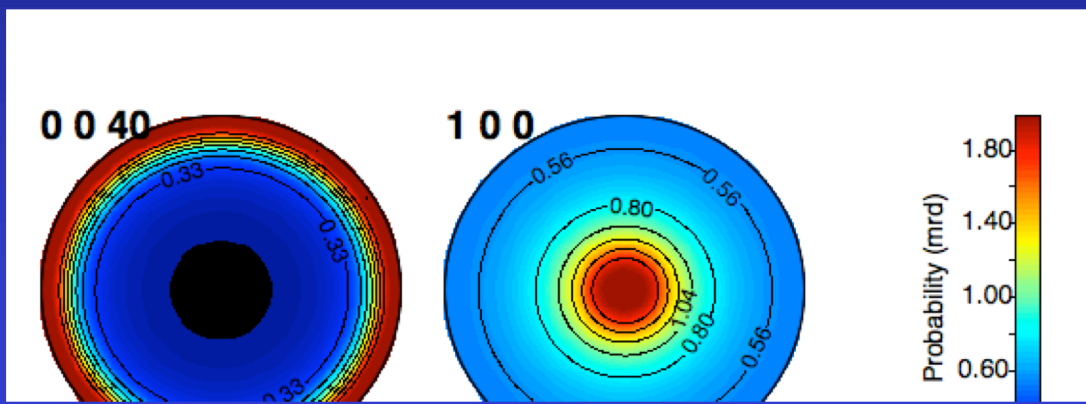
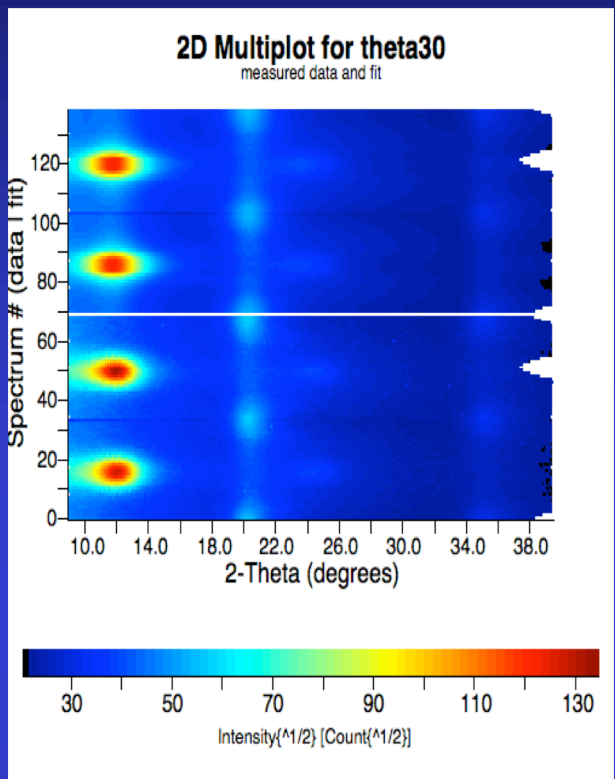


Carbon nanofibre



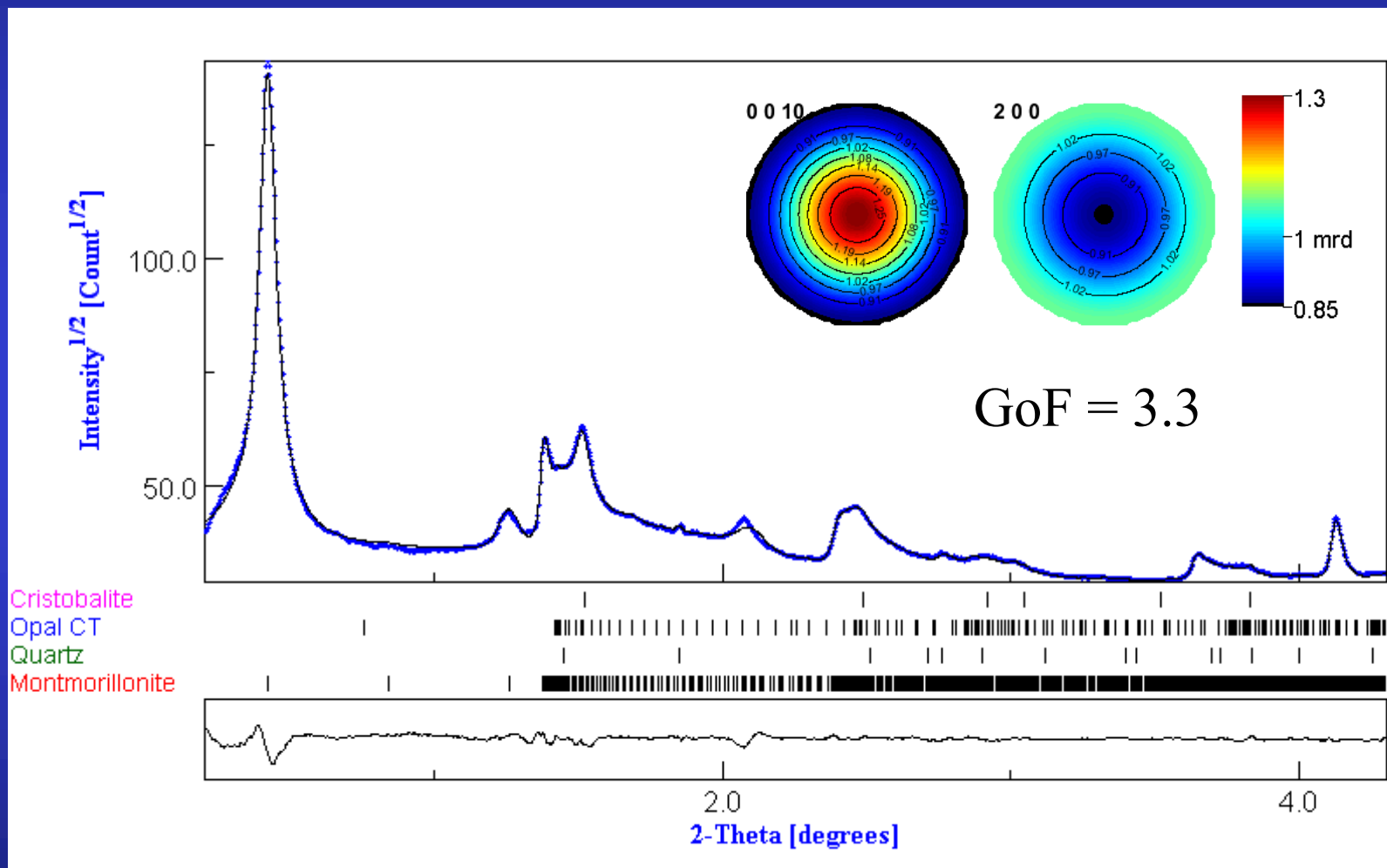
1 fibre (7 microns diameter): CCD Kappa diffractometer

Planar texture Component
Ufer turbostratic model

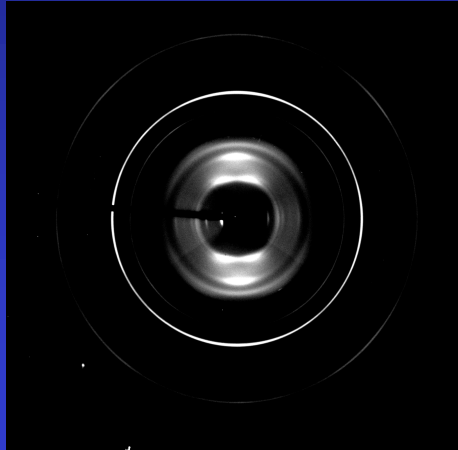


	A(nm)	C(nm)	Orientation FWHM(°)	Max 00l pole figure (m.r.d.)	Crystallite size along c (nm)	Crystallite size along a (nm)	Global microstrain (rms)
C1B1	0.23589(7)	0.6821(1)	21.6(1)	1.95	2.1(4)	2.2(4)	0.0152(10)
C2B1	0.23746(5)	0.68915(8)	18.75(6)	2.05	2.3(2)	2.5(2)	0.0154(11)
C3B1	0.23734(5)	0.69233(9)	18.63(6)	2.04	2.4(3)	2.7(5)	0.0136(6)
C3B2	0.23716(4)	0.69389(9)	19.87(7)	1.98	2.4(4)	2.5(4)	0.0150(4)
C3B3	0.23656(4)	0.68980(8)	19.16(6)	1.99	2.5(6)	2.3(5)	0.0168(8)

Turbostratic phyllosilicate aggregates

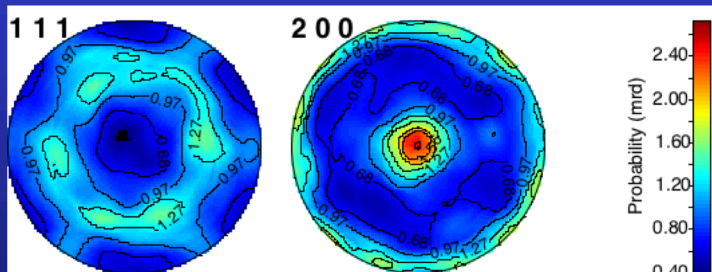
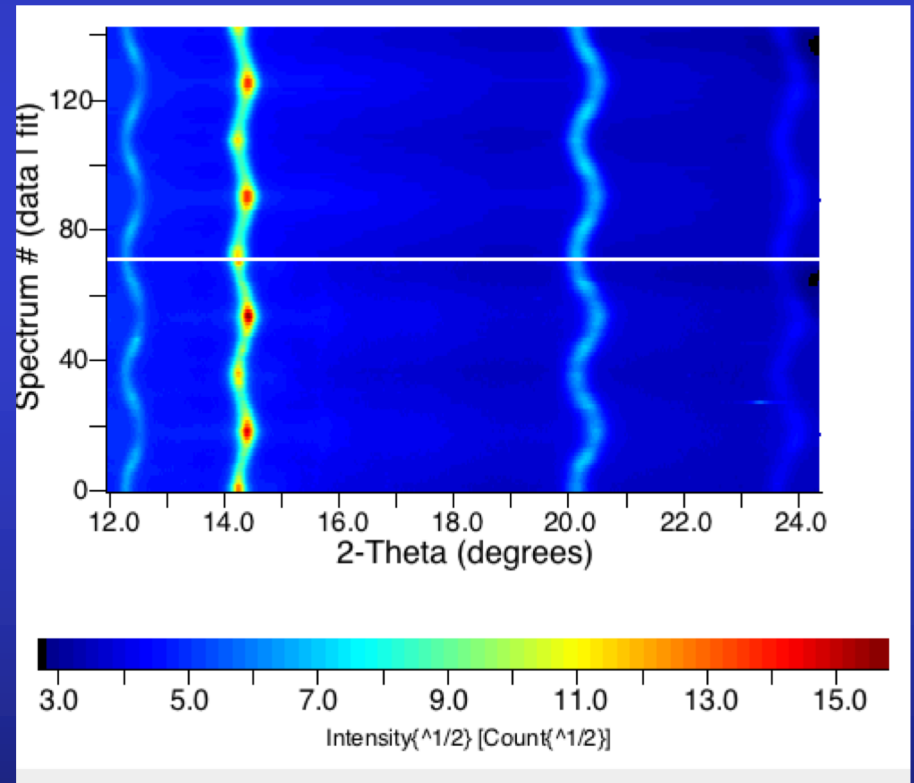


$Mg_{0.75}Fe_{0.25}O$ high pressure experiments



E-WIMV + geo

$a = 3.98639(3) \text{ \AA}$
 $\langle t \rangle = 46.8(3) \text{ \AA}$
 $\langle \epsilon \rangle = 0.00535(1)$
 $\sigma_{33} = -861(3) \text{ MPa}$



LiNbO₃

- Predict macroscopic anisotropic properties: BAW

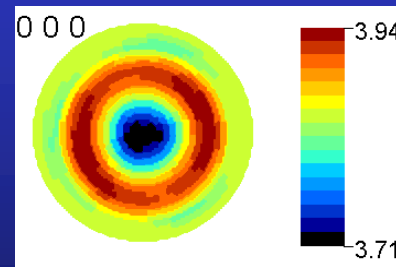
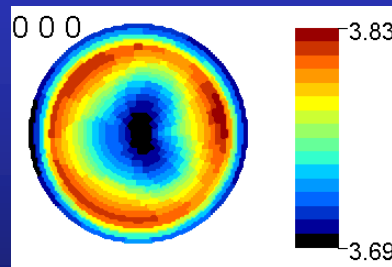
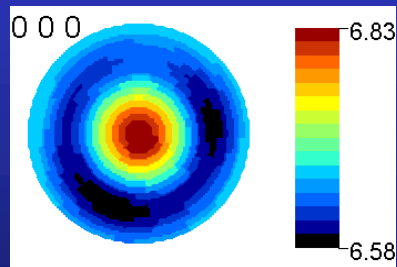
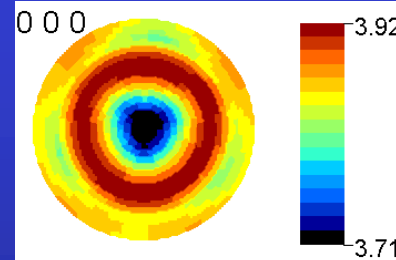
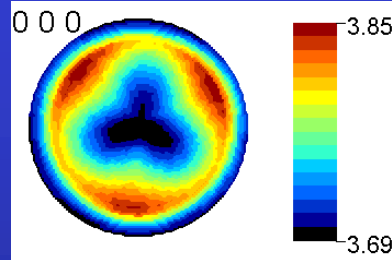
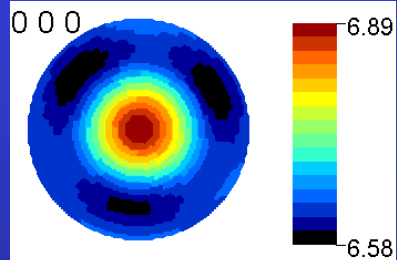
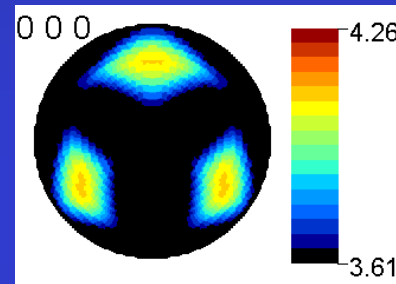
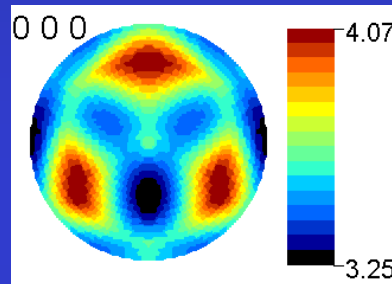
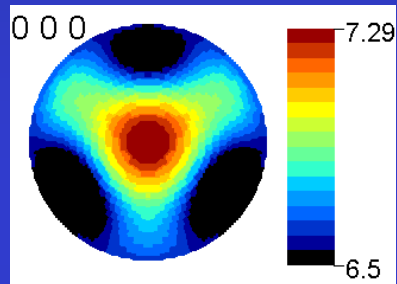
Propagation equation

$$\rho \frac{\partial^2 u^i}{\partial t^2} = \left[C^{i\ell mn} \right] \frac{\partial^2 u_n}{\partial x^m \partial x^\ell}$$

Propagation direction	V _P	V _{S1}	V _{S2}
[100]	$\sqrt{\frac{c^M_{11}}{\rho}}$	$\sqrt{\frac{c^M_{44}}{\rho}}$	$\sqrt{\frac{c^M_{44}}{\rho}}$
[110]	$\sqrt{\frac{c^M_{11} + 2c^M_{44} + c^M_{12}}{2\rho}}$	$\sqrt{\frac{c^M_{11} - c^M_{12}}{2\rho}}$	$\sqrt{\frac{c^M_{44}}{\rho}}$
[111]	$\sqrt{\frac{c^M_{11} + 4c^M_{44} + 2c^M_{12}}{3\rho}}$	$\sqrt{\frac{c^M_{11} + c^M_{44} - c^M_{12}}{3\rho}}$	$\sqrt{\frac{c^M_{11} + c^M_{44} - c^M_{12}}{3\rho}}$

Cubic crystal system

	c_{11} or c_{11}^M	c_{12} or c_{12}^M	c_{13} or c_{13}^M	c_{14} or c_{14}^M	c_{33} or c_{33}^M	c_{44} or c_{44}^M
Single crystal	201	54.52	71.43	8.4	246.5	60.55
LiNbO ₃ /Si	206.4	68.5	67.6	0.48	216.5	64
LiNbO ₃ /Al ₂ O ₃	204	65.7	69.7	1.1	219.9	63.2



Single crystal

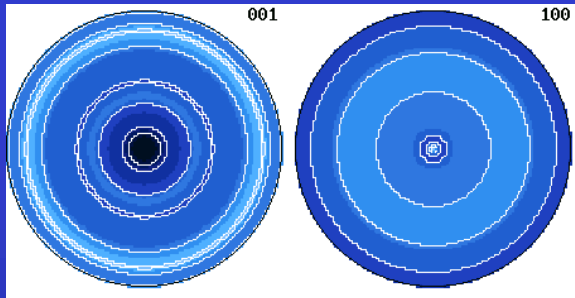
LiNbO₃/Si

LiNbO₃/Al₂O₃

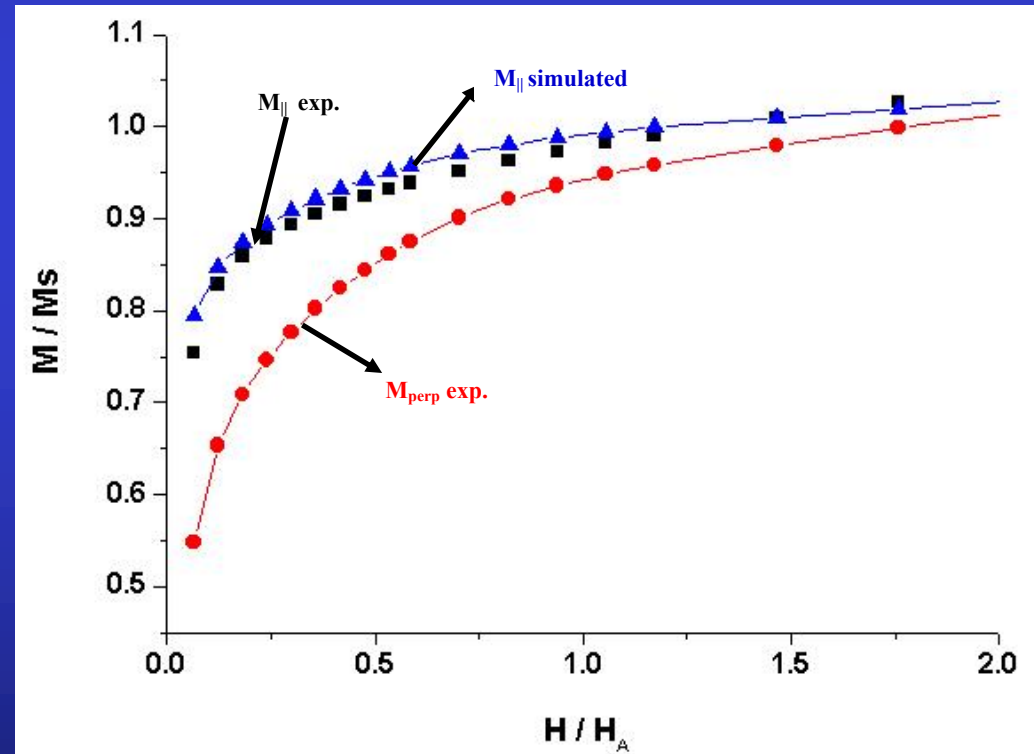
ErMn₃Fe₉C ferrimagnet

Predict macroscopic anisotropic properties: Magnetisation

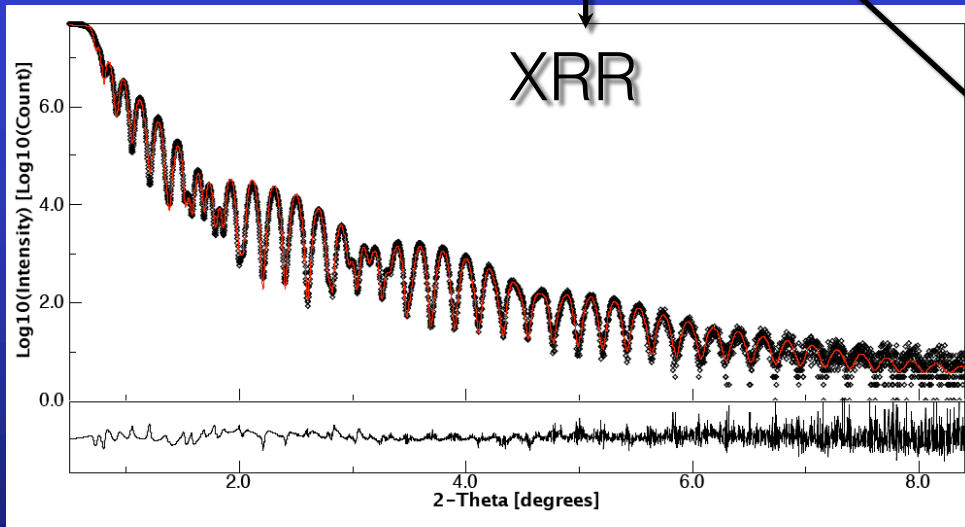
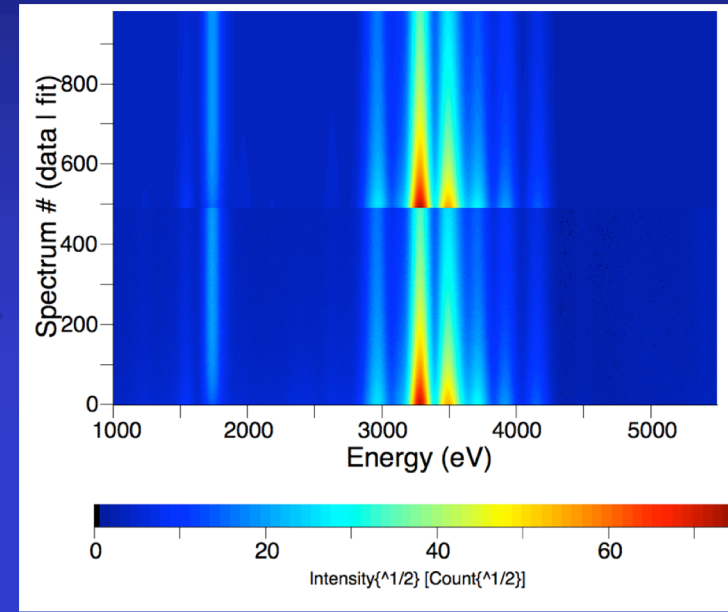
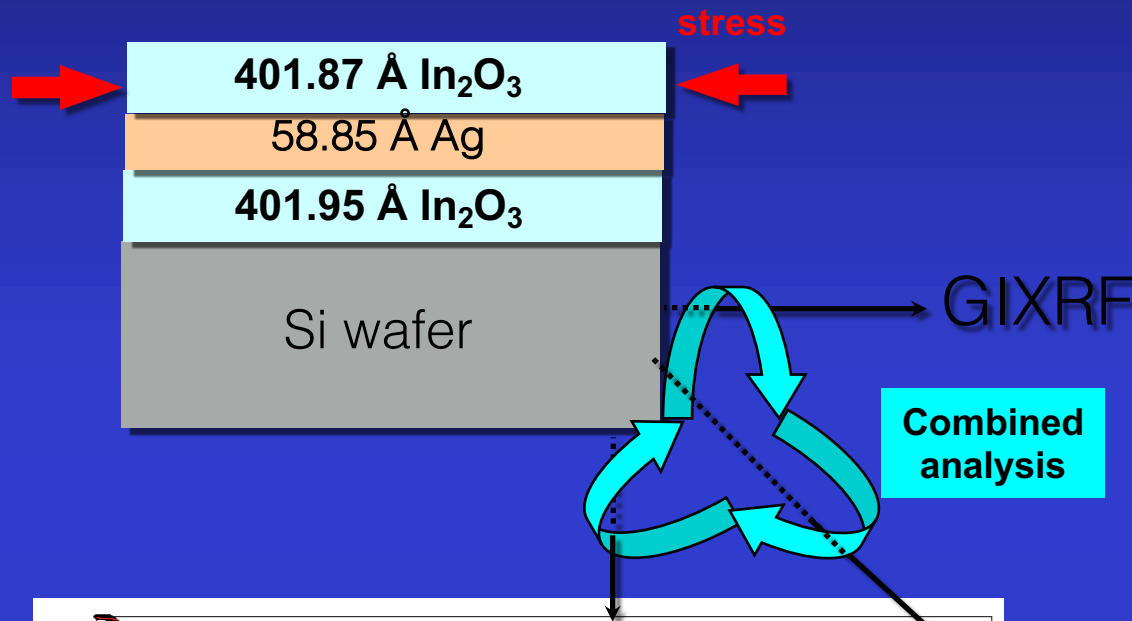
$$\frac{M_{\perp}}{M_S} = 2\pi \int_0^{\frac{\pi}{2}} (1 - \rho_0) PV(\theta_g) \sin\theta_g \cos(\theta_g - \theta) d\theta_g + \rho_0 M_{\text{random}}$$



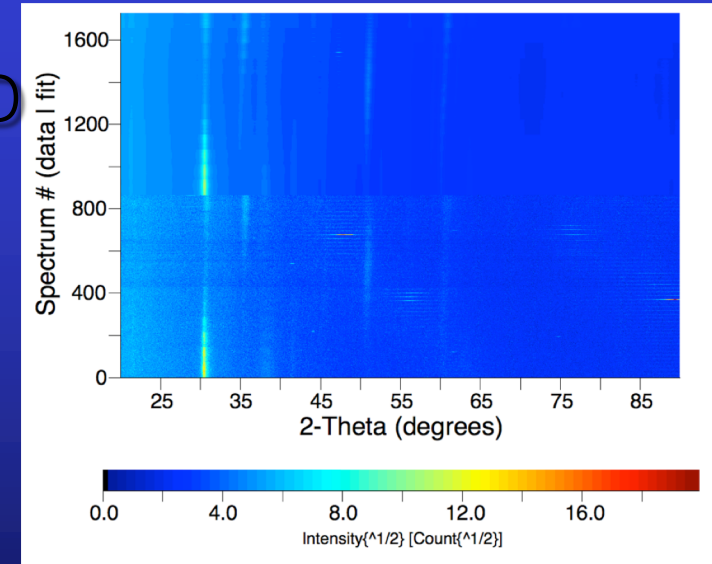
max {001}: 3.9 mrd
min: 0.5 mrd



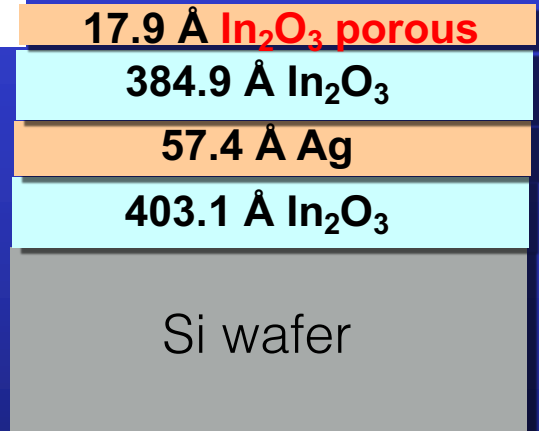
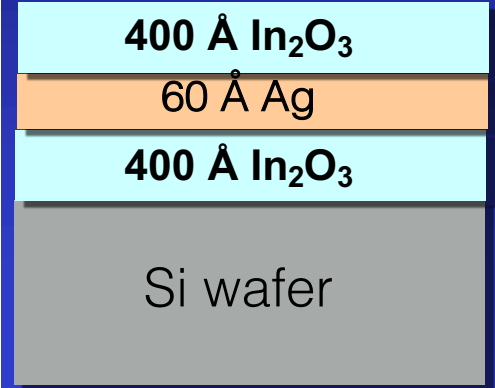
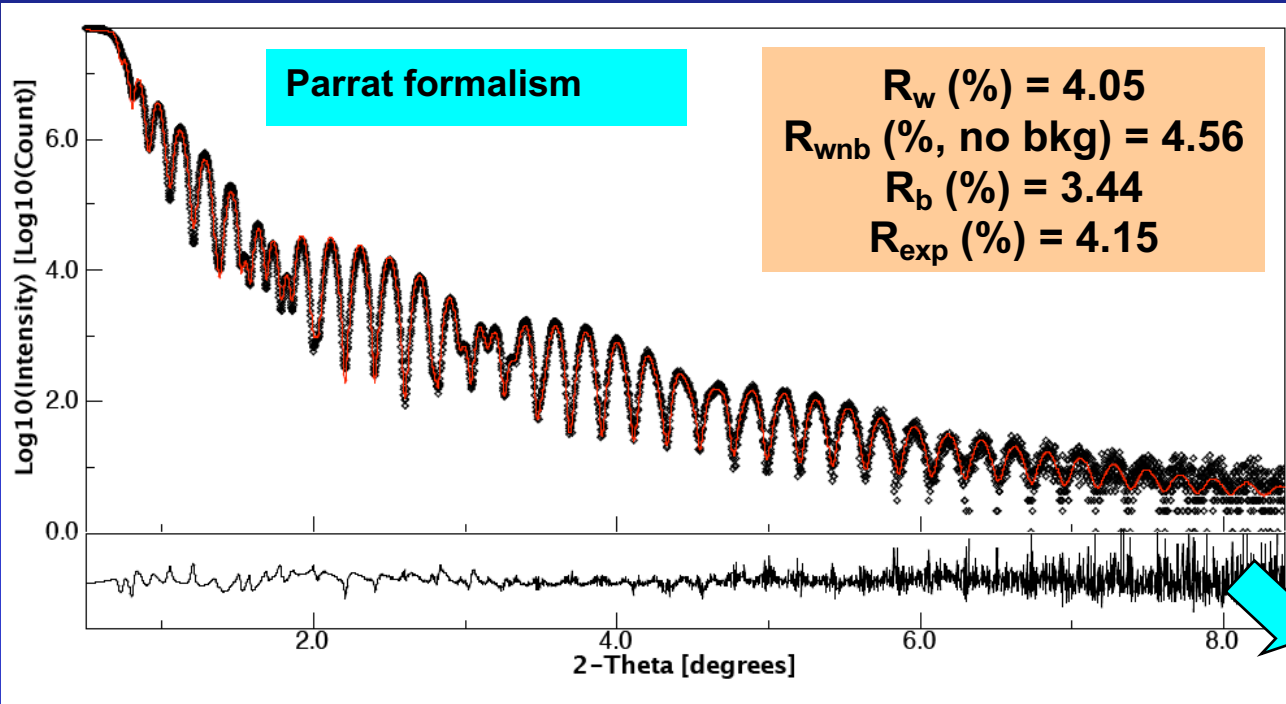
Combined XRR, XRD & GiXRF Analysis



XRD



XRR



Highly porous In_2O_3 layer

Top layer: $q_c = 0.0294 \text{ \AA}^{-1}$; roughness $r = 0.38 \text{ nm}$

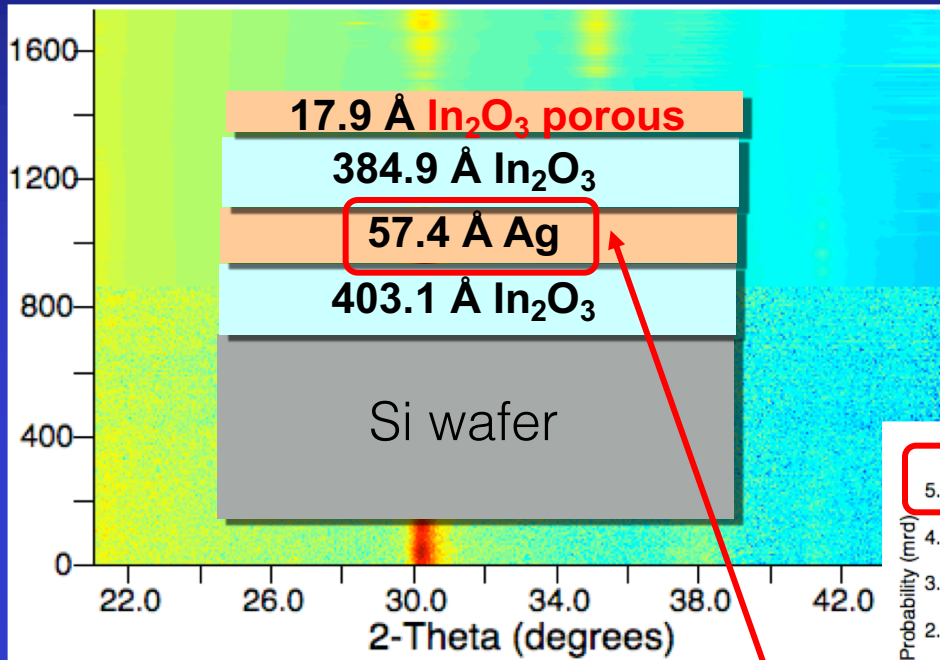
Top In_2O_3 : $q_c = 0.0504 \text{ \AA}^{-1}$; $r = 2.06 \text{ nm}$

Ag: $q_c = 0.0576 \text{ \AA}^{-1}$; $r = 0.26 \text{ nm}$

Bottom In_2O_3 : $q_c = 0.04889 \text{ \AA}^{-1}$; $r = 6.74 \text{ nm}$

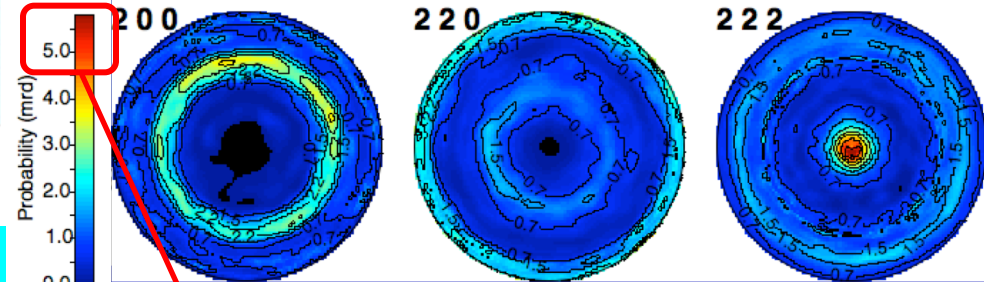
Si wafer: $q_c = 0.0313 \text{ \AA}^{-1}$; $r = 0.73 \text{ nm}$

XRD



R_w (%) = 23.97
 $R_{w\text{nb}}$ (% , no bkg) = 58.31
 R_b (%) = 18.71
 R_{exp} (%) = 22.04

In_2O_3



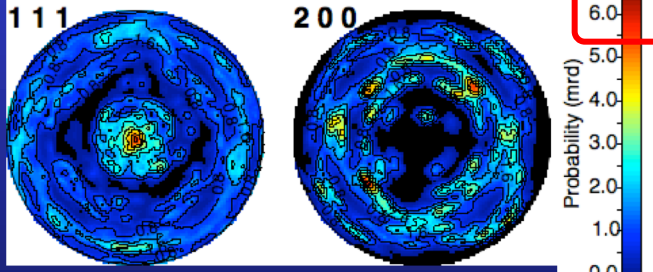
5 m.r.d.

Refined Ag phase parameters

↪ Isotropic crystallite size = 56.4 (1.3) Å

↪ Cell parameter: $a = 4.0943(7)$ Å

Ag:



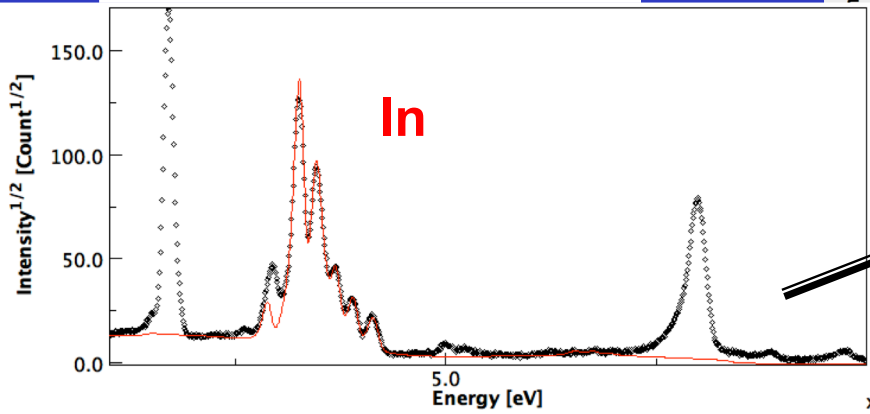
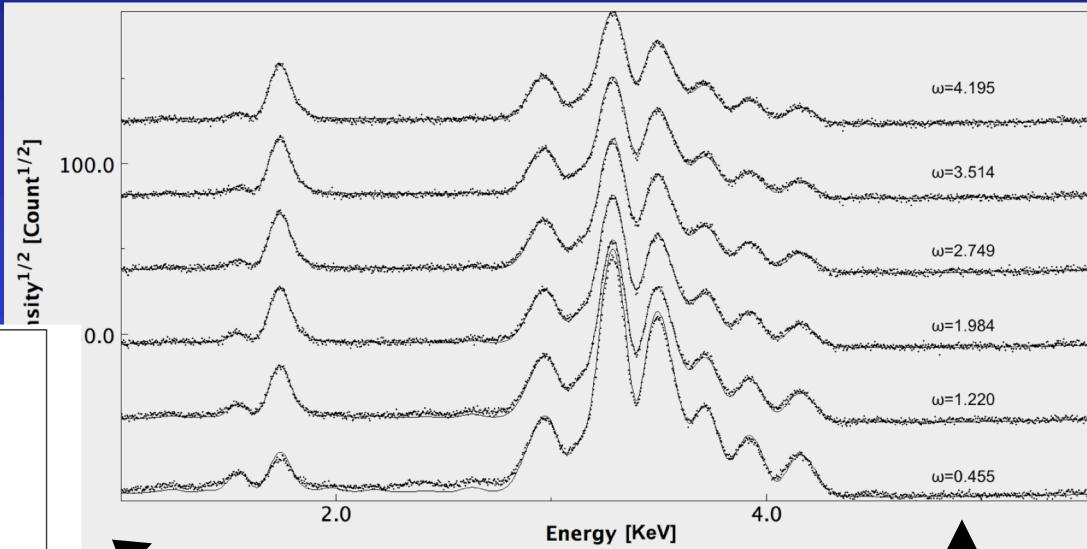
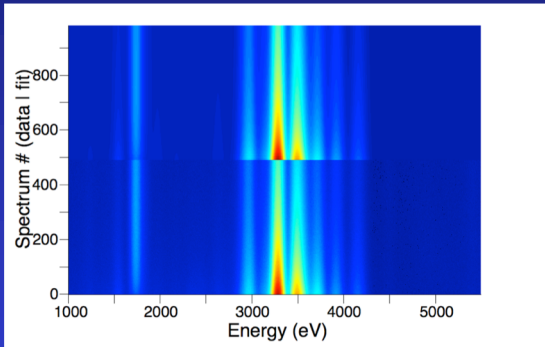
Refined In_2O_3 phase parameters

↪ $\sigma_{xx} = -1$ GPa (in-plane compressive stress)

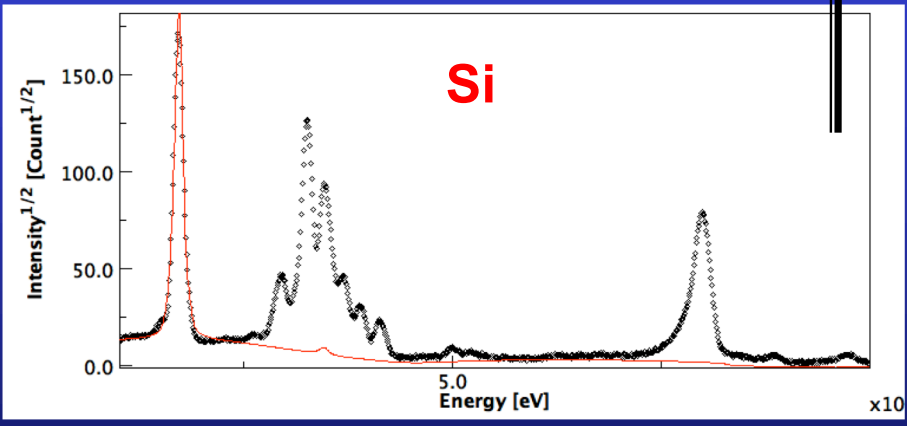
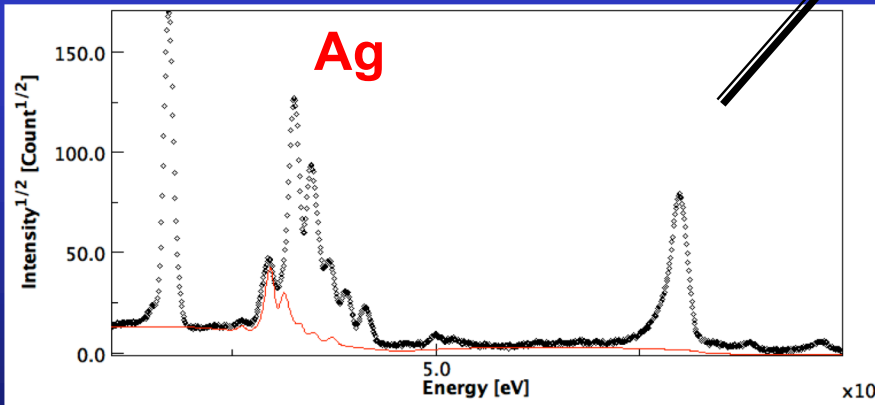
↪ Isotropic crystallite size = 153.2(5) Å

↪ Cell parameter: $a = 10.2104(5)$ Å

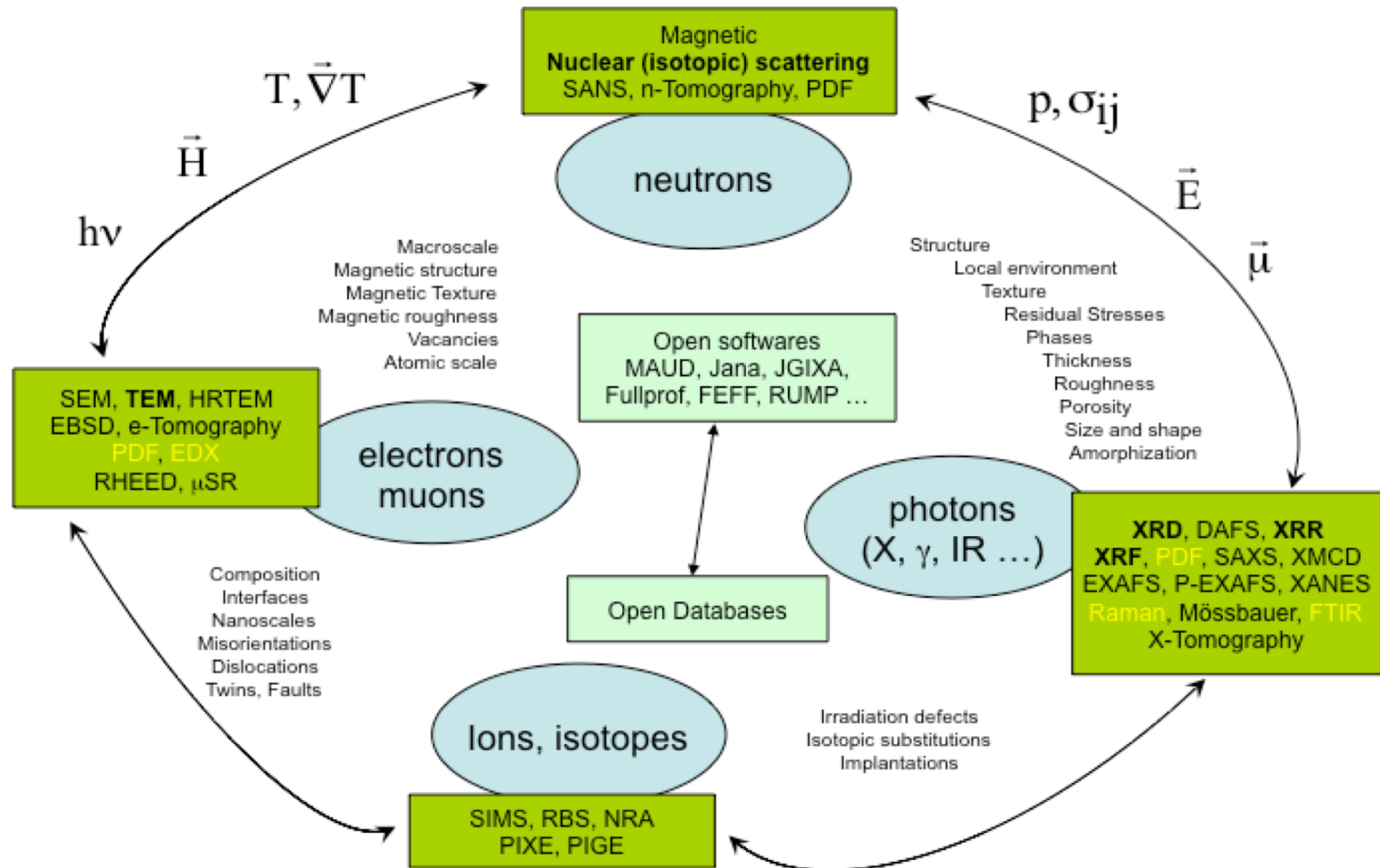
GiXRF



No presence of contaminant observed

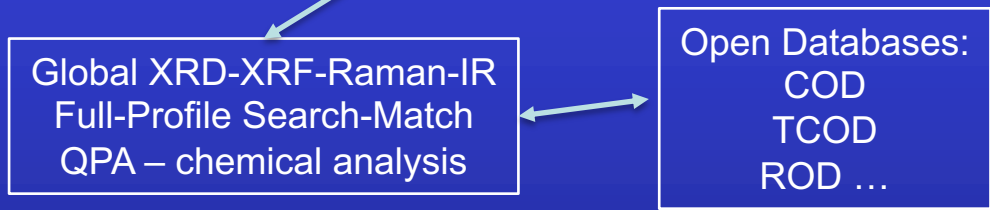
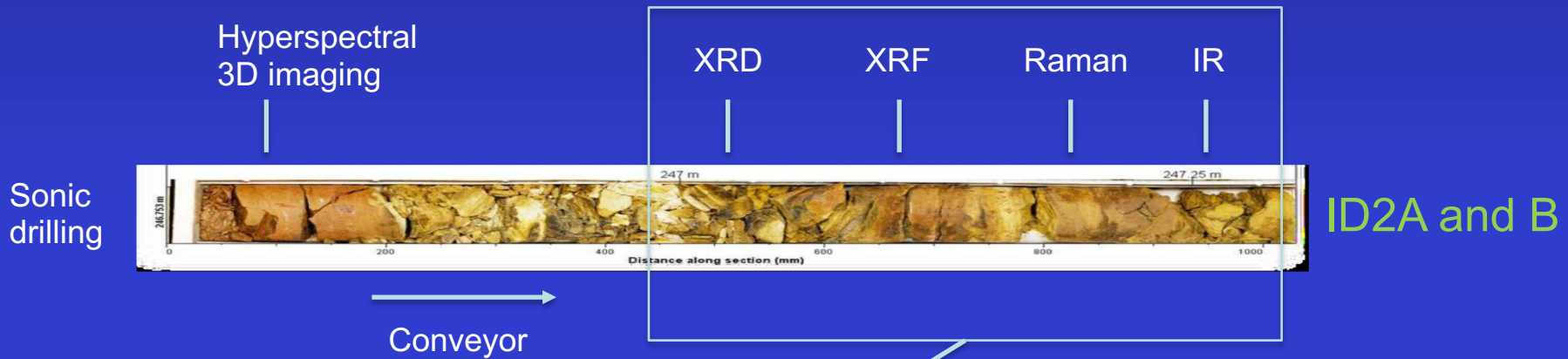


More ?



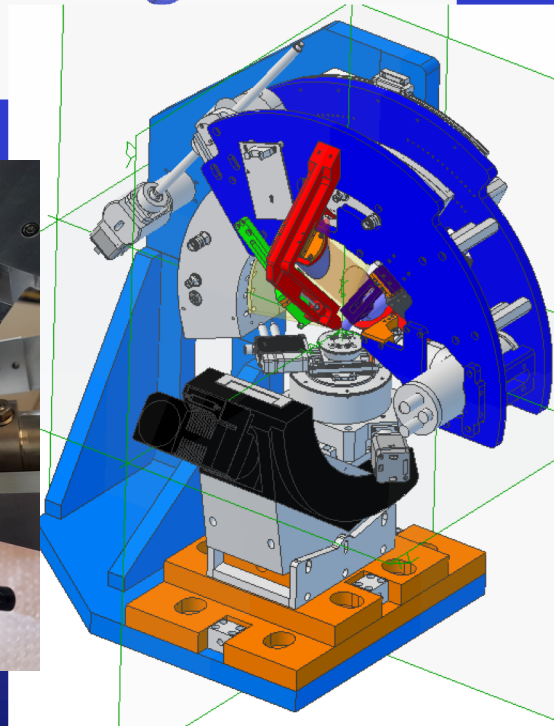
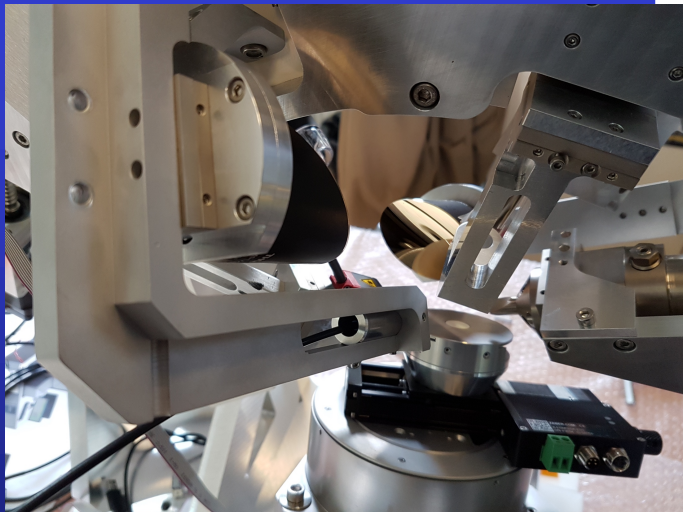
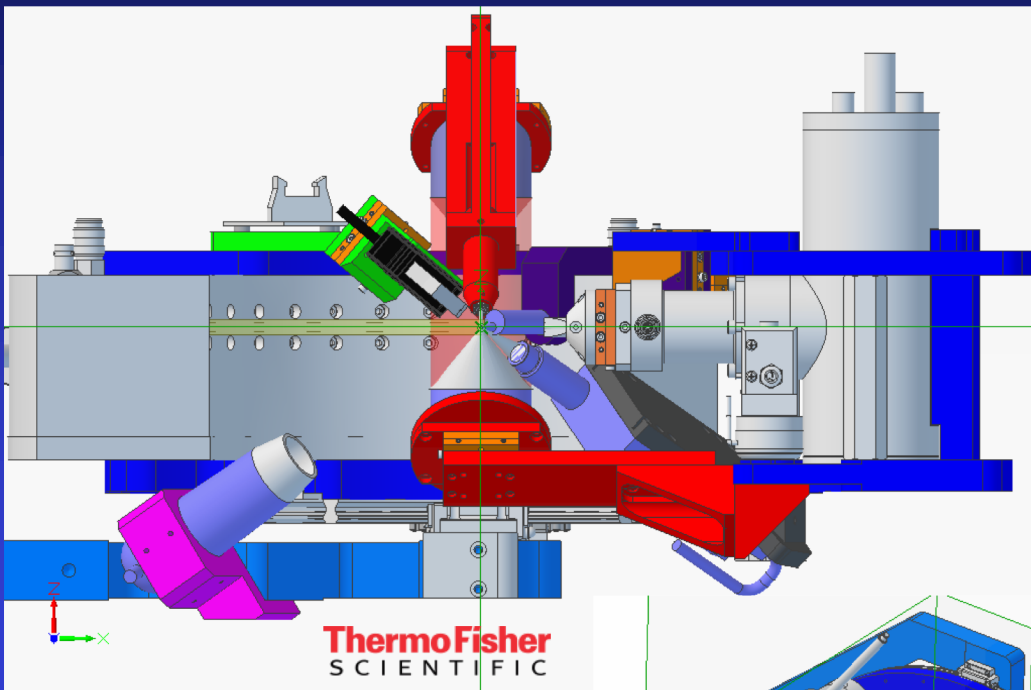
Combined Measurement-Analysis XRD-XRF-Raman for SOLSA

Sequential Acquisition (on-mine real-time)



Combined Analysis

or Combined Measurements and Analysis:  ID1




SOLSA
 Horizon 2020
 101018888

A 2016 Risk-oriented ESI-IRM Commitment
 Daniel CHATELAIN
 November 24, 2015
 Pierre-L. WELZEL

An innovative Expert System for
 Sustainable Exploration Technology & Geomodels
2016 - 2020

**SONIC DRILLING COUPLED WITH
 AUTOMATED MINERALOGY & CHEMISTRY
 ON MINE - ON LINE - REAL TIME**

European Mining and Metallurgical Industries need to secure the Metal Supply for our markets while minimizing environmental impact. SOLSA provides a breakthrough in combining drilling and analytical technologies. It will optimize exploration, resource and reserve estimates, mining and on-site process dysfunction.

CHALLENGES

- Lower grade, complex ores requiring multiple passes, high cost of drilling
- High level of automation and data collection
- Fluctuation in resource

COST-TIME REDUCTION on mine sites
 Tracer development for exploration & processing
 Optimizing resource and reserve estimates

EXPERT SYSTEM

- Robolized-automated semiquantitative drill core logging
- Reliable, validated mineralogical, textural & chemical data core-to-core-automated
- Based on Intelligent Big Analytical Data: mining & easy-to-use software
- Connect Drill Core parameters to logged data >> Up-grading the scientific open database (COD) for industrial purpose

2 Prototypes will be validated!

CONSORTIUM
 Nine transdisciplinary partners from 4 countries design and construct the expert system: 1 large and 2 small companies, 1 government organisation, 5 universities and 1 research institute.

GLOBAL BENEFITS
 SOLSA pushes Europe in front

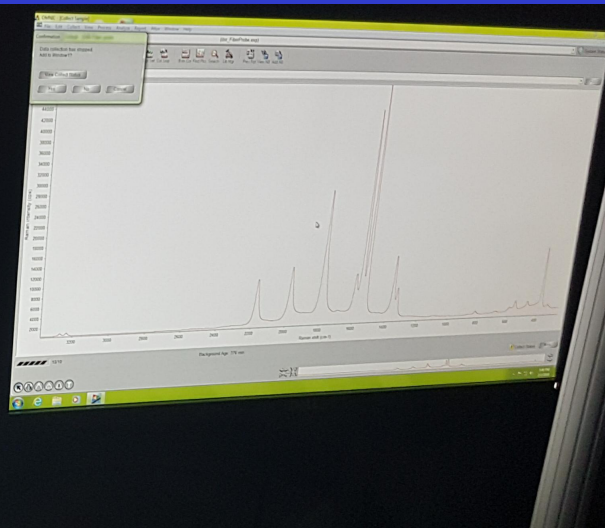
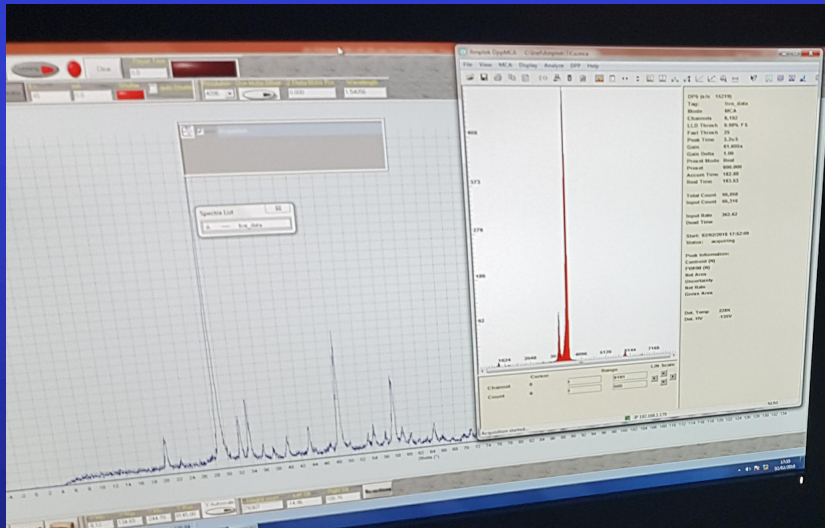
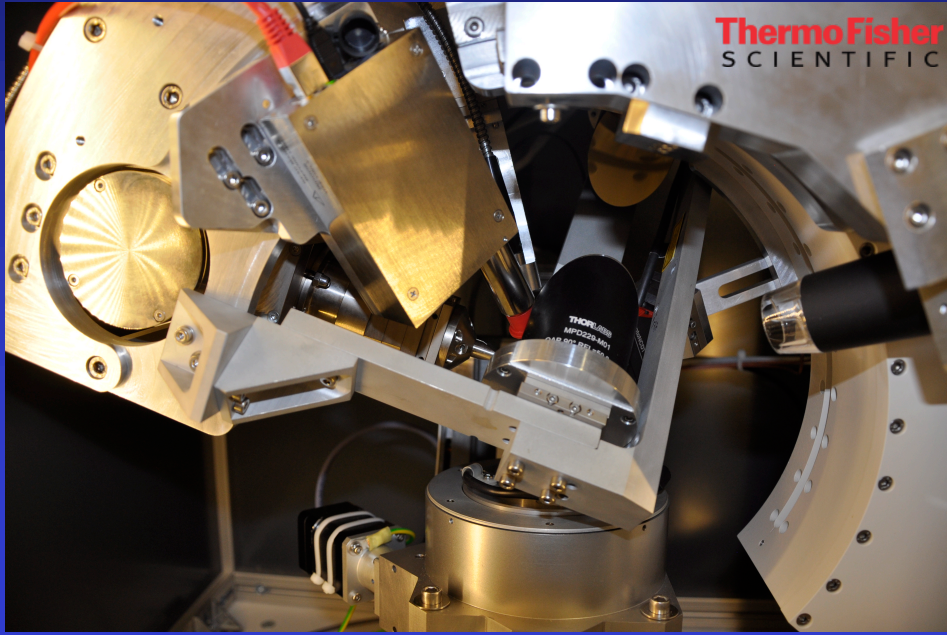
TASKS
 SOLSA will be implemented and operated in 2016-2017. The project will focus on the development of a new generation of drill core logging and analysis systems.

GLOBAL BENEFITS
 Knowledge transfer
 Education
 Job creation
 Mining
 Recycling
 Nuclear
 Optimal Mining

Total budget : 9.8 M€
 solsa@ict@evanetgroup.com



XRD-XRF-Raman-
 FTIR Combined
 Analysis (SOLSA
 EU projet)



XRD-
XRF-
Raman

Comb.
Meas.

XRD-XRF-Raman-IR Combined Analysis

$$I_{aj} = \frac{\lambda}{hc} C_{aj} \frac{\tau_{aj}}{\mu_{j\lambda}/\rho_j} J_{aj} \omega_a g_a \exp \left\{ - \sum_{n=1}^{j-1} \frac{\mu_{na} d_n}{\sin \Psi_d} \right\} S_1 \int_0^{d_j} dz \left(\frac{-\partial P_{jz}}{\partial z} \right) \exp \left(\frac{\mu_{ja} z}{\sin \Psi_d} \right)$$

IR

XRF-GiXRF- TXRF

EDS

Databases

COD-ROD-MPOD

Raman

XRR

$$I_{(e_s, e_0)} = I_0 \frac{\hbar}{2\omega_m} (n_m + 1) \frac{(\omega_0 - \omega_m)^4}{c^4} |e_s \cdot \alpha_{ij}^m \cdot e_0|^2$$

$$r = \frac{M_{12}}{M_{22}} = \frac{r_{01} + r_{12} e^{-2iq_{1z}h}}{1 + r_{01}r_{12} e^{-2iq_{1z}h}}$$


Diffraction extended Rietveld (n, X, e⁻)

$$y_c(\mathbf{y}_S, \theta, \eta) = y_b(\mathbf{y}_S, \theta, \eta) + I_0 \sum_{i=1}^{N_L} \sum_{\Phi=1}^{N_\Phi} \frac{v_i \Phi}{V_{c\Phi}} \sum_h L_p(\theta) j_{\Phi h} |F_{\Phi h}|^2 \Omega_{\Phi h}(\mathbf{y}_S, \theta, \eta) P_{\Phi h}(\mathbf{y}_S, \theta, \eta) A_{i\Phi}(\mathbf{y}_S, \theta, \eta)$$



Crystallography Open Database

COD Home

Home
What's new? 

Accessing COD Data

Browse
Search
Search by structural
formula

Add Your Data

Deposit your data
Manage depositions
Manage/release
prepublications

Documentation

COD Wiki
Obtaining COD
Querying COD
Citing COD
COD Mirrors
Advices to donators
Useful links



Open-access collection of crystal structures of organic, inorganic, metal-organic compounds and minerals, excluding [biopolymers](#).

Including data and [software](#) from [CrystalEye](#), developed by Nick Day at the [department of Chemistry](#), the University of Cambridge under supervision of [Peter Murray-Rust](#).

All data on this site have been placed in the public domain by the contributors.


COD Advisory Board thanks [The Research Council of Lithuania](#) for their financial support of the publication "[Crystallography Open Database \(COD\): an open-access collection of crystal structures and platform for world-wide collaboration](#)", *Nucleic Acids Research*. (2012) [PDF version](#)

We thank [Crystal Impact GbR](#) for their financial support of the publication "[Crystallography Open Database - an open-access collection of crystal structures](#)", *J. Appl. Crystallogr.* (2009) [PDF version](#)


Currently there are **379914** entries in the COD.
Latest deposited structure: [7228542](#) on **2017-06-26** at **09:50:13 UTC**

> 400,000 entries, fully freely downloadable

Grazulis et al. J. Appl. Cryst 2009



Raman Open Database

ROD Home
Home
What's new? 

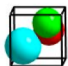
Accessing ROD Data
Search

Add Your Data
Deposit your data
Manage depositions
Manage/release
prepublications

Open-access collection of Raman spectra used for the [SOLSA H2020](#) project.

All data on this site have been placed in the public domain by the contributors.

Currently there are **1099** entries in the ROD.
Latest deposited structure: [3500265](#) on **2018-09-06** at **12:12:46 UTC**




Advisory Board

Lahfid Abdeltif, Mohamed-Ramzi Ammar, Jean-François Bardeau, Xavier Bourrat, Thanh Bui, Daniel Chateigner, Cédric Dué, Yassine El Mendili, Stephanie Gascoin, Saulius Gražulis, Bernard Hehlen, Marc Jeannin, Arun Kumar, Monique Le Guen, Charles Le Losq, Gino Mariotto, Nicolas Maubec, Andrius Merkys, Beate Orberger, Sébastien Petit, Henry Pilliere, Andrea Sanson, Maria Secchi, Patrick Simon, Adolfo Speghini, Antanas Vaitkus, Marco Zanatta


If you find bugs in the ROD or have any feedback, please contact us at
cod-bugs@ibt.lt

Acknowledgements

Raman Open Database has received funding from the European Union's Horizon 2020 research and innovation program under grant agreement No. 689868



Raman Open Database

ROD Home
Home
What's new? 


Accessing ROD Data
Search

Add Your Data
Deposit your data
Manage depositions
Manage/release
prepublications

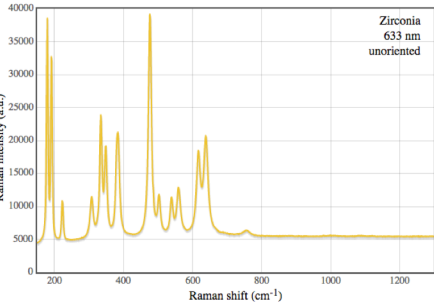
Information card for entry [3500265](#)

[3500264](#) << [3500265](#) >> [4020000](#)

Preview



Display in Jmol



Raman intensity (a.u.)

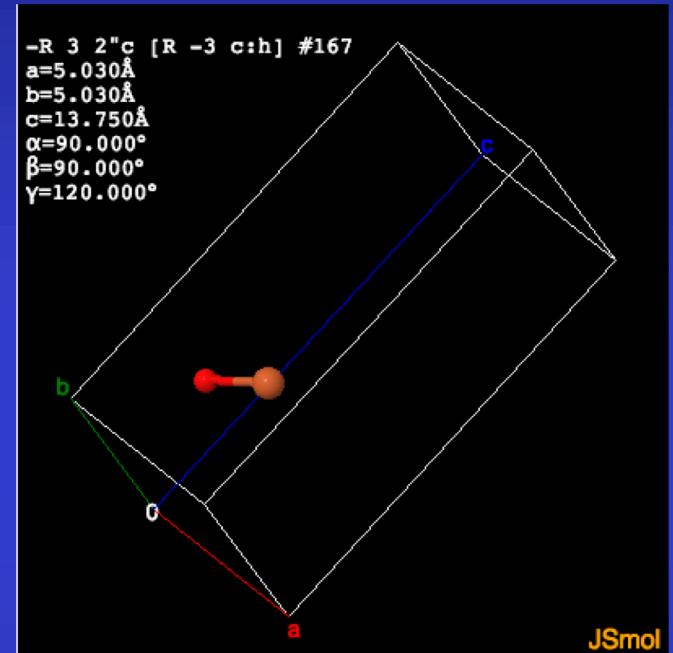
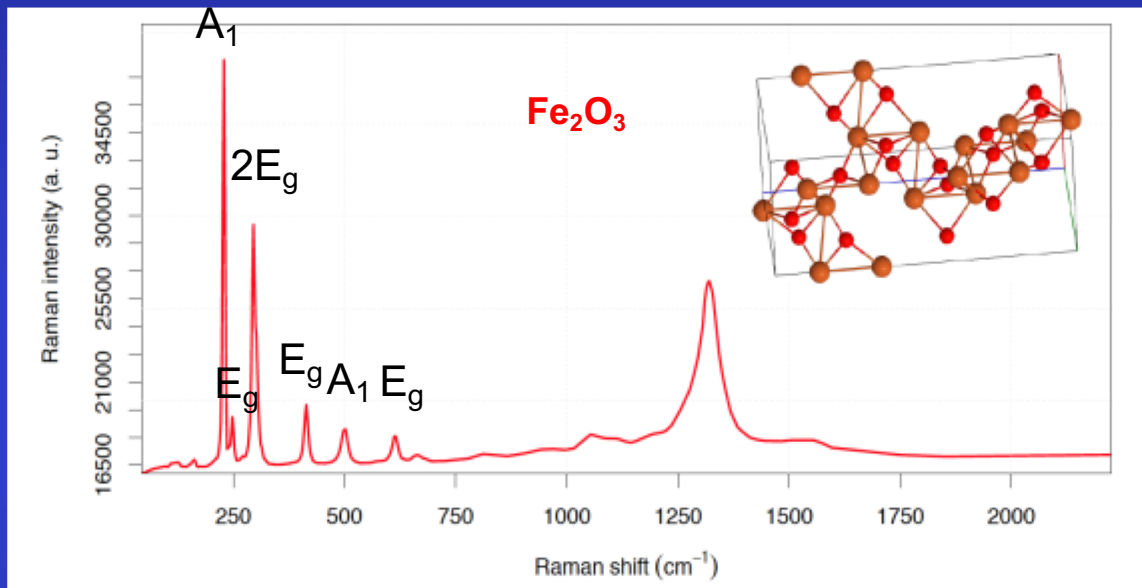
Raman shift (cm⁻¹)

Zirconia
633 nm
unoriented

Raman spectrum [3500265.rod](#) [3500265.xls](#)
External links
COD: [2300544](#)

Currently the database contains 1099 entries in the standard CIF and JCAMP-DX formats with data related to over than 780 different phases

COD \leftrightarrow ROD



ROD ID 1000002 \leftrightarrow COD ID 1546383

Y. El Mendili et al., J. Appl. Cryst. 2019

Full-Pattern Search-Match

[http://nanoair.dii.unitn.it:8080/sfpm/
cod.iutcaen.unicaen.fr](http://nanoair.dii.unitn.it:8080/sfpm/cod.iutcaen.unicaen.fr)

Diffraction pattern and sample composition

Upload diffraction pattern:

Atomic elements in the sample:

Sample nanocrystalline

Experiment details

Radiation:

X-ray tube:

Other : Wavelength (Å):

Instrument geometry:

Bragg-Brentano (theta-2theta)

Bragg-Brentano (2theta only), omega:

Debye-Scherrer

Transmission

Instrument broadening function:

Extra output (for debugging)

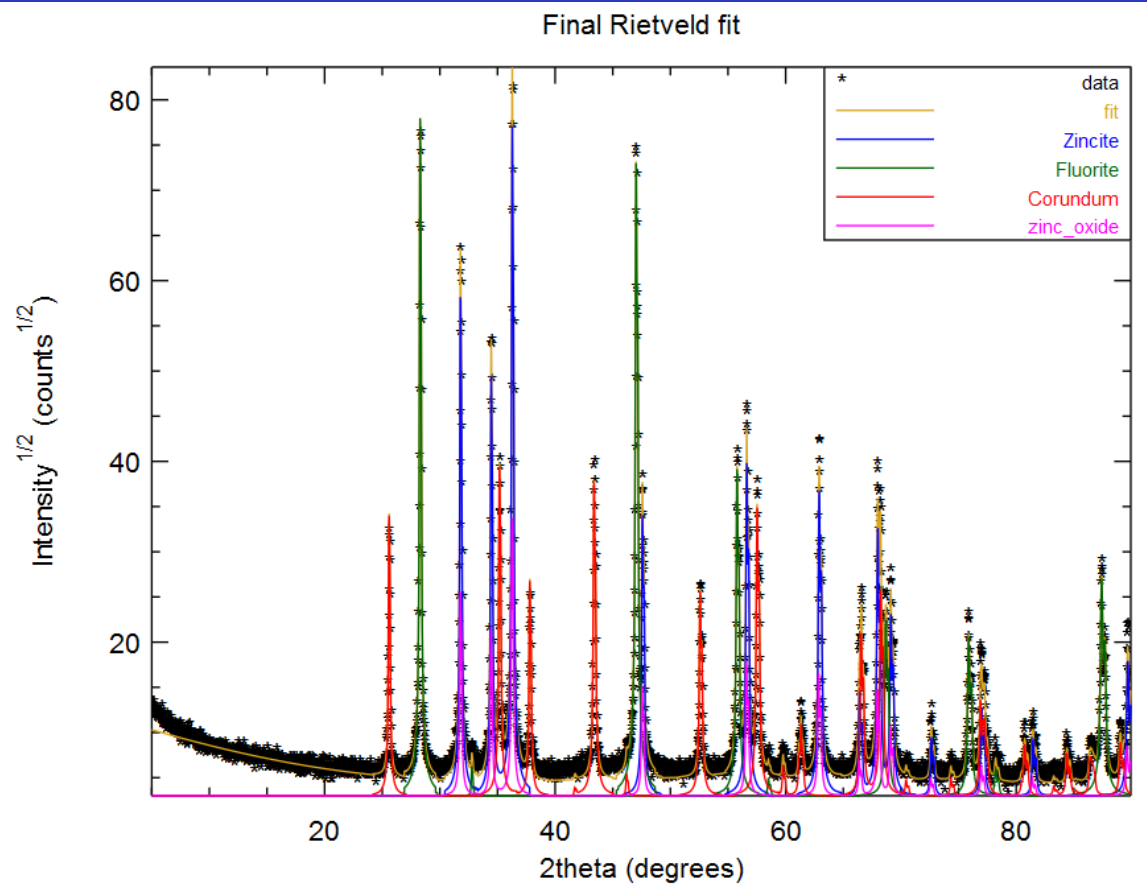
Structures database:

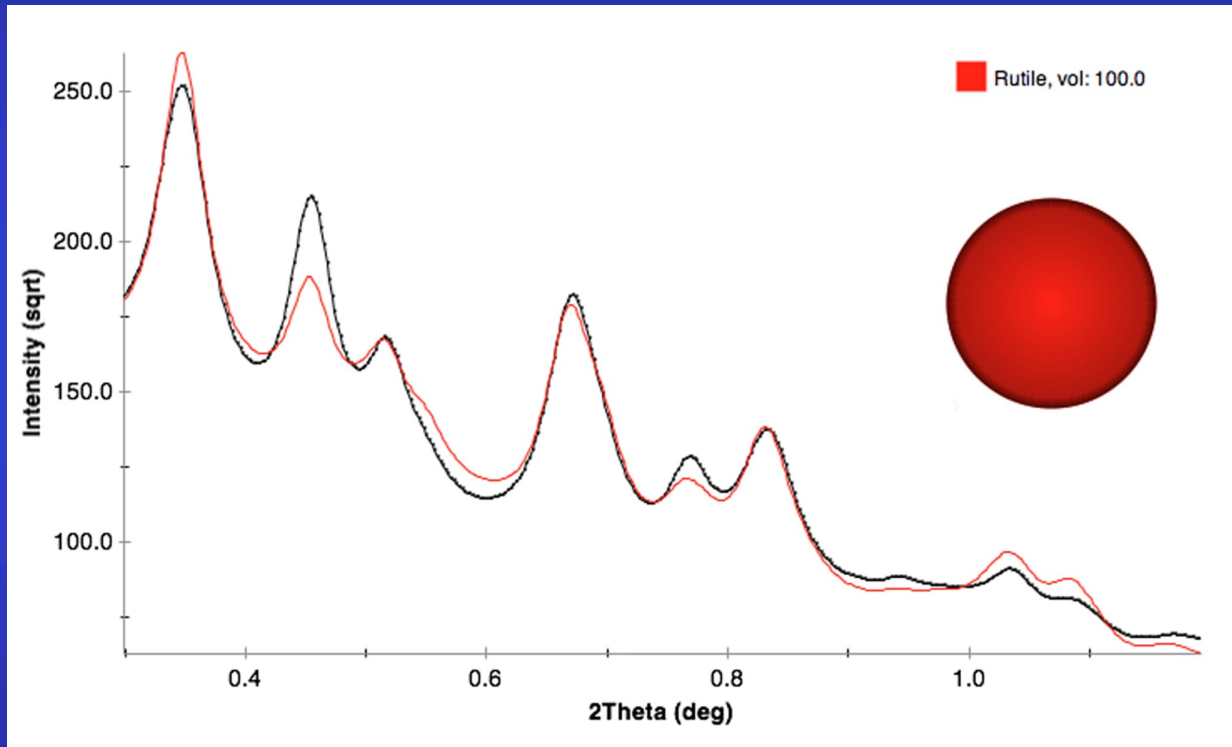
1 min later
>275000 COD
structures

Found phases and quantification:

Phase ID	name	vol. (%)	wt. (%)	crystallites (Å)	microstrain
9004178	Zincite	16.8284	23.9708	2148.26	0.00028435
9009005	Fluorite	42.5522	33.9388	2117.08	0.000363147
9007498	Corundum	37.2197	37.2493	1889.82	0.000267779
2300112	zinc_oxide	3.39971	4.84114	1754.74	6.98311e-05

Final Rietveld analysis, R_w: 0.159468, GofF: 1.95869





Rutile nanocrystalline Electron Powder Diffraction pattern

Combined Analysis Workshop series:

Next one in Caen 1st - 6th July 2019

www.ecole.ensicaen.fr/~chateign/formation/

Thanks !



ESQUI
SOLSA

MEET
MIND
Xmat
COSTs



COMBIX: Chair of Excellence



FURNACE
ECOCORAIL

DAME
SEMOME



SMAM